SELF-SIMILAR SINGULARITY OF A 1D MODEL FOR THE 3D AXISYMMETRIC EULER EQUATIONS

THOMAS Y. HOU AND PENGFEI LIU

Abstract. We investigate the self-similar singularity of a 1D model for the 3D axisymmetric Euler equations, which approximates the dynamics of the Euler equations on the solid boundary of a cylindrical domain. We prove the existence of a discrete family of self-similar profiles for this model and analyze their far-field properties. The self-similar profiles we find are consistent with direct simulation of the model and enjoy some stability property.

1. Introduction and Main Results

Whether the 3D Euler equations develop finite-time singularity is regarded as one of the most important open problems in mathematical fluid mechanics, and interested readers may consult the surveys [13, 2, 9] and references therein for more historical background about this outstanding problem. In this paper we investigate the self-similar singularity of a 1D model for the 3D axisymmetric Euler equations, which approximates the dynamics of the axisymmetric Euler equations on the solid boundary of a cylindrical domain. It is hoped that this work may help to analyze the singularity of the 3D Euler equations.

The investigated model is motivated by the numerical computation of Luo and Hou [21]. In that computation the 3D axisymmetric Euler equations [22] are solved in a cylinder,

$$u_{1,t} + u^r u_{1,r} + u^z u_{1,z} = 2u_1\phi_{1,z}, \tag{1.1a}$$

$$w_{1,t} + u^r w_{1,r} + u^z w_{1,z} = (u_1^2)_z, \tag{1.1b}$$

$$-[\partial_r^2 + (3/r)\partial_r + \partial_z^2]\phi_1 = w_1, \tag{1.1c}$$

where $u^r = -r\phi_{1,z}$, $u^z = 2\phi_1 + r\phi_{1,r}$ are radial and axial velocity, and $u_1 = u^\theta/r$, $w_1 = w^\theta/r$, $\phi_1 = \phi^\theta/r$ are transformed angular velocity, vorticity and stream function respectively.

According to the numerical results reported in [21], the solutions to (1.1) develop self-similar singularity in the meridian plane for certain initial conditions with no flow boundary condition at $r = 1$. The solid boundary and special symmetry of u^θ, ω^θ and ψ^θ in the axial direction seem to make the flow in the meridian plane remain hyperbolic near the singularity point and be responsible for the observed finite-time singularity. A 1D model which approximates the dynamics of the 3D axisymmetric Euler equations along the solid boundary of the cylindrical domain $r = 1$ has been proposed and investigated by Hou and Luo in [15]. The finite-time singularity of this model is proved very recently by Choi, Hou, Kiselev, Luo, Sverak and Yao in [6]. Motivated by the new singularity formation scenario in [21], Kiselev and Sverak [17] constructed an example of 2D Euler solutions in a setting similar to [21] and proved that the gradient of vorticity exhibits double exponential growth in time, which is known to be the fastest possible rate of growth for the 2D Euler equations. This example provides further evidence that the new singularity formation scenario reported in [21] is an interesting candidate to investigate the 3D Euler singularity.

Thomas Y. Hou, hou@cms.caltech.edu. Pengfei Liu, plliu@caltech.edu.

Inspired by the work of [15] and [17], Choi, Kiselev and Yao proposed the following 1D model (we call it the CKY model for short) [7] on $[0,1]$:

$$\partial_t w + u\partial_x w = \partial_x \theta, \tag{1.2a}$$

$$\partial_t \theta + u\partial_x \theta = 0, \tag{1.2b}$$

$$u(x,t) = -x\int_x^1 \frac{w(y,t)}{y}\mathrm{d}y, \tag{1.2c}$$

$$w(0,t) = 0, \quad \theta(0,t) = 0, \quad \partial_x\theta(0,t) = 0. \tag{1.2d}$$

This 1D model can be viewed as a simplified approximation to the 1D model proposed by Hou and Luo in [15], and its finite-time singularity from smooth initial data has been proved in [7]. Like the 1D model of Hou and Luo, the CKY model approximates the 3D axisymmetric Euler equations (1.1) on the boundary of the cylinder $r = 1$ with

$$\theta \sim u_1^2, \quad w \sim w_1, \quad u \sim u^z. \tag{1.3}$$

The positivity of $\theta_x(x,t)$ near the origin creates a compressive flow which is responsible for the finite-time singularity of this model (1.2), and we will use this fact in our construction in section 2. Numerical simulation suggests that this model develops finite-time singularity in a way similar to that of the 3D axisymmetric Euler equations on the boundary of the cylinder [21]. Moreover, the singular solutions to this model also appear to develop self-similar structure. The main purpose of this paper is to prove the existence of self-similar singular solutions to this CKY model from smooth initial data.

We make the following self-similar ansatz to the local singular solutions,

$$\theta(x,t) = (T-t)^{c_\theta}\Theta\left(\frac{x}{(T-t)^{c_l}}\right), \tag{1.4a}$$

$$u(x,t) = (T-t)^{c_u}U\left(\frac{x}{(T-t)^{c_l}}\right), \tag{1.4b}$$

$$w(x,t) = (T-t)^{c_w}W\left(\frac{x}{(T-t)^{c_l}}\right). \tag{1.4c}$$

Plugging these self-similar ansatz into equations (1.2) and matching the exponents of $(T-t)$ for each equation, we get

$$c_w = -1, \quad c_u = c_l - 1, \quad c_\theta = c_l - 2. \tag{1.5}$$

And the self-similar profiles $U(\xi)$, $W(\xi)$, $\Theta(\xi)$ satisfy the following equations defined on $\mathbf{R}^+$,

$$(2-c_l)\Theta(\xi) + c_l\xi\Theta'(\xi) + U(\xi)\Theta'(\xi) = 0, \tag{1.6a}$$

$$W(\xi) + c_l\xi W'(\xi) + U(\xi)W'(\xi) - \Theta'(\xi) = 0, \tag{1.6b}$$

$$U(\xi) = -\xi\int_\xi^\infty \frac{W(\eta)}{\eta}\mathrm{d}\eta. \tag{1.6c}$$

According to (1.2d), we require the following boundary condition for the profiles at $\xi = 0$

$$W(0) = 0, \quad \Theta(0) = 0, \quad \Theta'(0) = 0. \tag{1.7a}$$

If we assume that the finite-time singularity of this CKY model is an isolated point singularity, as we have observed in our numerical simulation, then the ansatz (1.4) requires the

following matching condition for the self-similar profiles at infinity,

$$\Theta(\xi) \sim O(\xi^{1-2/c_l}), \quad W(\xi) \sim O(\xi^{-1/c_l}), \quad U(\xi) \sim O(\xi^{1-1/c_l}), \quad \xi \to +\infty. \tag{1.7b}$$

We refer equations (1.6) as the self-similar equations, which can be easily verified to enjoy the following scaling-invariant property:

$$U(\xi) \to \frac{1}{\lambda} U(\lambda\xi), \quad W(\xi) \to W(\lambda\xi), \quad \Theta(\xi) \to \frac{1}{\lambda}\Theta(\lambda\xi), \quad \lambda > 0. \tag{1.8}$$

In this paper we investigate the solutions to the self-similar equations (1.6). A key fact for the CKY model is that the velocity and the vorticity field satisfy a local relation (1.9c), and the self-similar equation is equivalent to the following ODE system

$$(2 - c_l)\Theta(\xi) + c_l\xi\Theta'(\xi) + U(\xi)\Theta'(\xi) = 0, \tag{1.9a}$$

$$W(\xi) + c_l\xi W'(\xi) + U(\xi)W'(\xi) - \Theta'(\xi) = 0, \tag{1.9b}$$

$$\left(\frac{U(\xi)}{\xi}\right)' = \frac{W(\xi)}{\xi}, \tag{1.9c}$$

with a decay condition

$$\lim_{\xi \to +\infty} \frac{U(\xi)}{\xi} = 0. \tag{1.10}$$

We first ignore the decay condition (1.10) and consider the ODE system (1.9) which has a singularity at the origin since the coefficients of the first order derivatives vanish at $\xi = 0$. We confine ourselves to analytic solutions of (1.9), and use the power series method to construct the manifold of local solutions. We prove that for fixed c_l and leading order of $\Theta(\xi)$ at the origin, there exist unique (up to rescaling) analytic solutions to the singular ODE system, and these local solutions can be extended to the whole $\mathbf{R}^+$ through the ODE system (1.9). Then we show that the decay condition (1.10) determines the scaling exponent c_l, and there exist a discrete family of c_l, corresponding to different leading orders of $\Theta(\xi)$, to make the constructed self-similar profiles satisfy the decay condition (1.10). We achieve this with the assistance of numerical computation and rigorous error control. Given the decay condition (1.10), we further analyze the far-field properties of the constructed self-similar profiles and show that they satisfy the desired matching condition (1.7b) at infinity.

Our main result is the following theorem:

Theorem 1.1. *There exist a discrete family of scaling exponents c_l (determined by the decay condition* (1.10)*), such that the self-similar equations* (1.6) *have analytic solutions $U(\xi), W(\xi), \Theta(\xi)$ with boundary and far-field conditions* (1.7)*. This family of solutions correspond to different leading orders of $\Theta(\xi)$ at the origin, $s = 2, 3, \ldots$, where*

$$s = \min\{k \in N^+ | \ \frac{\mathrm{d}^k}{\mathrm{d}\xi^k}\Theta(0) \neq 0\}. \tag{1.11}$$

Moreover, $W(\xi)$, $U(\xi)\xi^{-1}$, $\Theta(\xi)\xi^{-1}$ are analytic with respect to $\zeta = \xi^{-1/c_l}$ at $\zeta = 0$.

Remark 1.1. *We only consider analytic self-similar profiles in our construction, thus our results do not rule out possible existence of self-similar profiles that are non-analytic.*

An interesting fact for this model is that self-similar profiles (1.6) exist for a discrete set of scaling exponent c_l, corresponding to different leading orders of $\Theta(\xi)$. We also find that these self-similar profiles are consistent with direct simulation of the 1D model and enjoy some

stability property in the sense that for fixed leading order of $\theta(x,0)$, the singular solutions using different initial conditions converge to the same set of self-similar profiles.

The self-similar profiles we construct are non-conventional in the sense that the velocity does not decay to zero at infinity but grows with certain fractional power. As a result, the velocity field at the singularity time is Hölder continuous. Such behavior was also observed in the numerical simulation of the 3D Euler equations in [15], which is very different from the Leray type of self-similar solutions of the 3D Euler equations, whose existence has been ruled out under certain decay assumptions on the self-similar profiles [4, 3, 5].

Our method of analysis is of interest by itself. The existence result relies on the use of a power series method to deal with the singularity of the self-similar equations at the origin, and some very subtle and relatively sharp estimates of the self-similar profiles. The same approach can be taken to analyze the self-similar singularity of Burgers equation and get results similar to those obtained in this paper. However, the method of analysis presented in this paper does not generalize directly to study the singularity formation of the full 3D Euler equations. Due to the global nature of the Biot-Savart law for the 3D Euler equations, we need a new set of techniques to control the nonlinear interaction terms.

Another novelty in our analysis is the use of numerical computation with rigorous error control, which is an important step in establishing the existence of self-similar solutions. Our strategy to rigorously control the numerical error, including the truncation error of the integration scheme for an ODE system and the roundoff error introduced due to floating point operation, is quite general and can be used for other purposes.

The rest of this paper is organized as follows. In section 2, we construct the local self-similar profiles using a power series method and extend them to the whole $\mathbf{R}^+$. In section 3, we show that the decay condition in the Biot-Savart law determines the scaling exponents in the self-similar solutions. In section 4, we prove the existence of self-similar profiles for different leading orders of $\Theta(\xi)$ at the origin. In section 5, we analyze the far-field behavior of the self-similar profiles. In section 6, we present our numerical results.

2. Construction of the Near-field Solutions

In this section, we ignore the decay condition (1.10) and use a power series method to construct the manifold of local analytic solutions to (1.9). We also show that these local solutions can be extended to the whole $\mathbf{R}^+$ through (1.9).

The use of power series to analyze analytic differential equations is classical, and can be traced back to the Cauchy-Kowalevski Theorem [18, 11]. At a regular point of an ODE system, the manifold of local solutions can be parametrized by the initial values of the solution [8]. For the non-linear system (1.9), we consider its analytic solutions near a singular point (the origin), and show that the manifold of local analytic solutions can be parameterized by the values of the leading order of $\Theta(\xi)$. We have the following theorem.

Theorem 2.1. *For fixed $c_l > 2$, and leading order of $\Theta(\xi)$, $s \geq 2$, there exist a unique (up to rescaling) local analytic solution to* (1.9) *with boundary condition* (1.7a).

Proof. According to the boundary condition of the self-similar profiles (1.7a), we assume

$$\Theta(\xi) = \sum_{k=2}^{\infty} \Theta_k \xi^k, \quad U(\xi) = \sum_{k=1}^{\infty} U_k \xi^k, \quad W(\xi) = \sum_{k=1}^{\infty} W_k \xi^k. \tag{2.1a}$$

Based on the local relation in the Biot-Savart law (1.9c), we have

$$W_k = kU_{k+1}. \tag{2.1b}$$

Plugging (2.1) into (1.9) and matching the k-th ($k \geq 1$) order term ξ^k, we get

$$(2-c_l)\Theta_k + kc_l\Theta_k + \sum_{m=1}^{k-1}(k-m+1)\Theta_{k-m+1}U_m = 0, \tag{2.2a}$$

$$(k-1)U_k + c_l(k-1)^2U_k + \sum_{m=1}^{k-1}U_m(k-m)^2U_{k-m+1} - k\Theta_k = 0. \tag{2.2b}$$

Note that if initially the leading order of $\theta(x,0)$ at the origin is s, then according to (1.2b), s will remain as the leading order of the solution $\theta(x,t)$ as long as the velocity field is smooth. Correspondingly we assume that the leading order of $\Theta(\xi)$ at the origin is s (1.11). As we have discussed in section 1, $\partial_x\theta(x,t)$ should be positive near $x=0$ to produce finite-time singularity, so in the corresponding self-similar profile (2.1a), we require that

$$\Theta_i = 0 \text{ for } i < s, \quad \Theta_s > 0, \quad s \geq 2. \tag{2.3}$$

To make (2.2a) hold for $1 \leq k \leq s$, we require

$$(2 - c_l + sc_l + sU_1)\Theta_s = 0. \tag{2.4}$$

Since $\Theta_s \neq 0$, we require

$$U_1 = \frac{(1-s)c_l - 2}{s}. \tag{2.5}$$

To make (2.2b) hold for $2 \leq k < s$, we require

$$[(k-1) + c_l(k-1)^2 + U_1(k-1)^2]U_k = 0. \tag{2.6}$$

Since $c_l > 2$, and $[(k-1) + c_l(k-1)^2 + U_1(k-1)^2] > 0$, we require

$$U_k = 0, \quad 1 < k < s. \tag{2.7}$$

And to make (2.2b) hold for $k = s$, we require

$$U_s = \frac{s^2\Theta_s}{(sc_l - c_l - s + 2)(s-1)} > 0. \tag{2.8}$$

For $k > s$, to make (2.2) hold, the coefficients Θ_k and U_k should satisfy

$$\Theta_k = \frac{-\sum_{m=s}^{k-1}U_m(k-m+1)\Theta_{k-m+1}}{(k/s-1)(c_l-2)}, \tag{2.9a}$$

$$U_k = \frac{k\Theta_k - \sum_{m=s}^{k-1}U_m(k-m)^2U_{k-m+1}}{(k-1) + (c_l/s - 2/s)(k-1)^2}, \tag{2.9b}$$

which means the power series (2.1) can be determined inductively.

To complete the proof, we need to verify that the constructed power series (2.1) converge for ξ small enough. We choose $u^0, \theta^0, r > 0$ such that the following condition holds

$$|U_s| \leq \frac{1}{s^2}u^0r^s, \quad |\Theta_s| \leq \frac{1}{s}\theta^0r^s, \quad \frac{(s+1)u^0r}{c_l/s - 2/s} \leq 1, \quad \frac{9}{4}\frac{\theta^0/u^0 + u^0r}{c_l/s - 2/s} < 1. \tag{2.10}$$

We can achieve this by choosing u_0r and θ_0/u_0 small enough to make the last two hold, and then choosing r large enough to make the first two hold. For example, let

$$A = \min\{\frac{c_l-2}{s(s+1)}, \frac{2(c_l-2)}{9s}\}, \ B = \frac{2(c_l-2)}{9s}, \ C = \max\{\frac{s\Theta_s}{AB}, \frac{s^4\Theta_s}{A(sc_l - c_l - s + 2)}\}. \tag{2.11}$$

Then the choice of

$$u^0 = \frac{A}{C^{1/(s-1)}}, \quad \theta^0 = u^0 B, \quad r = C^{1/(s-1)}, \tag{2.12}$$

will satisfy (2.10). And we will use induction to prove that for all $k \geq s$,

$$|U_k| \leq \frac{1}{k^2} u^0 r^k, |\Theta_k| \leq \frac{1}{k} \theta^0 r^k. \tag{2.13}$$

For $k = s$, (2.13) holds by (2.10). Assume now that for $s \leq k < n$, (2.13) holds, then for $k = n \geq s+1$, based on (2.9a) we have

$$|\Theta_n| \leq \frac{\sum_{m=s}^{n-1} |U_m||(n-m+1)||\Theta_{n-m+1}|}{(n-s)(c_l/s - 2/s)}. \tag{2.14}$$

Using the induction assumption and the fact that $\sum_{m=2}^{\infty} \frac{1}{m^2} \leq 1$, we have

$$|\Theta_n| \leq \frac{\theta^0 u^0 r^{n+1}}{(n-s)(c_l/s - 2/s)} \leq \frac{\theta^0 r^n}{n} \times \frac{(s+1)u^0 r}{c_l/s - 2/s} \leq \frac{\theta^0 r^n}{n}, \tag{2.15}$$

where we have used the fact $n \geq s+1$ in the second inequality and (2.10) in the third inequality. Thus (2.13) holds for Θ_n. Based on (2.9b), we have

$$|U_n| \leq \frac{|n\Theta_n| + \sum_{m=s}^{n-1} |U_m (n-m)^2||U_{n-m+1}|}{(c_l/s - 2/s)(n-1)^2} \tag{2.16}$$

Using the induction assumption and the fact that $\sum_{m=2}^{\infty} \frac{1}{m^2} \leq 1$, we get

$$|U_n| \leq \frac{\theta^0 r^n + (u^0)^2 r^{n+1}}{(c_l/s - 2/s)(n-1)^2} \leq \frac{u_0 r^n}{n^2} \times \frac{\theta_0/u_0 + u_0 r}{c_l/s - 2/s} \times \frac{n^2}{(n-1)^2} \leq \frac{u_0 r^n}{n^2}, \tag{2.17}$$

where we have used (2.10) and the fact that $n \geq 3$, $n^2/(n-1)^2 \leq 9/4$ in the last inequality.

So we get that (2.13) holds by induction, which implies that the power series (2.1) converge in some interval $[0, 1/r)$. Note that we have one degree of freedom Θ_s (2.4) in constructing the power series solutions, which can be easily verified to play the same role as the rescaling parameter (1.8). With this we complete the proof of Theorem 2.1. □

Remark 2.1. *We require $c_l > 2$ in Theorem 2.1. If $c_l = 2$, there exist only trivial solutions to* (1.6)*. If $c_l < 2$, then $c_\theta < 0$ according to* (1.5)*, which means $\theta(x,t)$ blows up in finite time according to* (1.4)*. This is impossible since $\theta(x,t)$ is transported by the fluid* (1.2b)*.*

The power series (2.1) that we construct only converge in a short interval near $\xi = 0$. However, these local self-similar profiles can be extended to $+\infty$.

Theorem 2.2. *For $c_l > 2$, the analytic solutions* (2.1) *that we construct in Theorem 2.1 can be extended to the whole $\mathbf{R}^+$, resulting in global solutions to the ODE system* (1.9)*. Moreover, we have that for $\xi > 0$,*

$$W(\xi) > 0, \quad \Theta(\xi) > 0. \tag{2.18}$$

Proof. Since $c_l + U_1 = (c_l - 2)/s > 0$, $\Theta_s > 0$, $W_s = (s-1)U_s > 0$, based on the leading orders of the power series (2.1), we can choose $\epsilon < \frac{1}{r}$ small enough such that

$$c_l \epsilon + U(\epsilon) > 0, \quad W(\epsilon) > 0, \quad \Theta(\epsilon) > 0. \tag{2.19}$$

Then we consider extending the self-similar profiles from $\xi = \epsilon$ to $+\infty$ by solving the ODE system with initial conditions given by the power series (2.1). Let $\tilde{U}(\xi) = c_l\xi + U(\xi)$, then according to (1.9), $\tilde{U}(\xi)$, $\Theta(\xi)$ and $W(\xi)$ satisfy the following ODE system,

$$\Theta'(\xi) = \frac{(c_l - 2)\Theta(\xi)}{\tilde{U}(\xi)}, \tag{2.20a}$$

$$W'(\xi) = \frac{(c_l - 2)\Theta(\xi)}{\tilde{U}(\xi)^2} - \frac{W(\xi)}{\tilde{U}(\xi)}, \tag{2.20b}$$

$$(\frac{\tilde{U}(\xi)}{\xi})' = \frac{W(\xi)}{\xi}. \tag{2.20c}$$

The right hand side of (2.20) is locally Lipschitz continuous for $\tilde{U}(\xi) \neq 0$, $\xi \neq 0$, so we can solve the ODE system from ϵ and get its solutions on interval $[\epsilon, T)$. We first prove that $W(\xi)$ is positive on $[\epsilon, T)$. Otherwise denote $\xi = t$ as the first time $W(\xi)$ reaches 0, i.e.

$$t = \inf\{s \in [\epsilon, T) : W(s) \leq 0\}. \tag{2.21}$$

Then we have $W(\xi)$ is positive on $[\epsilon, t)$, and

$$W'(t) \leq 0. \tag{2.22}$$

Based on (2.20c), $\frac{\tilde{U}(\xi)}{\xi}$ is increasing on $[\epsilon, t)$, thus $\tilde{U}(\xi) > \tilde{U}(\epsilon) > 0$ for $\xi \in [\epsilon, t]$. Then based on (2.20a), $\Theta(\xi)$ is increasing on $[\epsilon, t]$, and $\Theta(t) > 0$. Evaluating (2.20b) at $\xi = t$, we get

$$W'(t) = \frac{(c_l - 2)\Theta(t)}{\tilde{U}(t)^2} > 0, \tag{2.23}$$

which contradicts with (2.22). So $W(\xi) > 0$ and consequently $\Theta(\xi) > 0$ for $\xi \in [\epsilon, T)$.

Using the fact that $W(\xi) > 0$ in (2.20c), we have that for $\xi > \epsilon$,

$$\tilde{U}(\xi) \geq C_0\xi. \tag{2.24}$$

Using this lower bound in (2.20a), we get

$$\Theta'(\xi) \leq \frac{C_1\Theta(\xi)}{\xi}. \tag{2.25}$$

This implies that for $\xi > \epsilon$

$$\Theta(\xi) \leq C_2\xi^{C_1}. \tag{2.26}$$

Using (2.26), (2.24) and the fact that $W(\xi)$ is positive in (2.20b), we have

$$W'(\xi) \leq C_3\xi^{C_1-2}. \tag{2.27}$$

Thus for $\xi > \epsilon$,

$$W(\xi) \leq C_4\xi^{C_1}. \tag{2.28}$$

Finally using (2.28) in (2.20c), we get that for $\xi > \epsilon$,

$$\tilde{U}(\xi) \leq C_5\xi^{C_1+1}. \tag{2.29}$$

The C_0, C_1,... C_5 in the above estimates are positive constants. These *a priori* estimates (2.24), (2.29), (2.26) and (2.28) together imply that we can get solutions to (2.20) on $[\epsilon, +\infty)$, i.e., the local self-similar profiles constructed using power series can be extended to $+\infty$. □

3. Determination of the Scaling Exponents

In constructing self-similar profiles in the previous section, we did not consider the decay condition (1.10). In this section, we show that the decay condition determines the scaling exponent c_l, i.e. only for certain c_l do the constructed self-similar profiles satisfy the decay condition. Recall that for fixed leading order of $\Theta(\xi)$, s and $\Theta_s = 1$, the constructed profiles $U(\xi)$, $\Theta(\xi)$ and $W(\xi)$ depend on c_l only. So we can define a function $G(c_l)$ as

$$G(c_l) = \lim_{\xi \to +\infty} \frac{U(\xi)}{\xi}. \tag{3.1}$$

We will prove that $G(c_l) < +\infty$ and it is a continuous function of c_l. Then the existence of c_l to make the decay condition (1.10) hold will follow from the Intermediate Value Theorem if we can show that there exist c_l^l and c_l^r such that

$$G(c_l^l) < 0, \quad G(c_l^r) > 0. \tag{3.2}$$

Theorem 3.1. *For fixed $c_l > 2$ and leading order of $\Theta(\xi)$, $s \geq 2$, construct the power series (2.1) with $\Theta_s = 1$, and extend the profiles to $\mathbf{R}^+$ by solving (2.20). Then*

$$G(c_l) = \lim_{\xi \to \infty} \frac{U(\xi)}{\xi} < +\infty, \tag{3.3}$$

and $G(c_l)$ is a continuous function of c_l.

We first make the following change of variables,

$$\eta = \xi^{1/c_l}, \quad \hat{W}(\eta) = W(\xi), \quad \hat{U}(\eta) = U(\xi)\xi^{-1}, \quad \hat{\Theta}(\eta) = \Theta(\xi)\xi^{-1+2/c_l}. \tag{3.4}$$

Then we have

$$G(c_l) = \lim_{\eta \to +\infty} \hat{U}(\eta), \tag{3.5}$$

and the ODE system satisfied by $\hat{U}(\eta), \hat{\Theta}(\eta), \hat{W}(\eta)$ is

$$\hat{\Theta}'(\eta) = \frac{(2/c_l - 1)\hat{\Theta}(\eta)\hat{U}(\eta)}{\eta + 1/c_l \hat{U}(\eta)\eta}, \tag{3.6a}$$

$$\hat{W}'(\eta) = \frac{-\hat{W}(\eta)}{\eta + 1/c_l \hat{U}(\eta)\eta} + \frac{(1 - 2/c_l)\hat{\Theta}(\eta)}{(1 + 1/c_l \hat{U}(\eta))^2 \eta^3}, \tag{3.6b}$$

$$\hat{U}'(\eta) = \frac{c_l \hat{W}(\eta)}{\eta}. \tag{3.6c}$$

According to (2.5), (2.18) and the fact that $\hat{U}(\eta)$ is monotone increasing, we have

$$\hat{U}(\eta) > \hat{U}(0) = \frac{(1-s)c_l - 2}{s}, \quad \hat{W}(\eta) > 0, \quad \hat{\Theta}(\eta) > 0, \quad \text{for} \quad \eta > 0. \tag{3.7}$$

Before proving Theorem 3.1, we will first prove the following two lemmas.

Lemma 3.1. *For all $c_l > 2$, $G(c_l) > -2$.*

Proof. Assume that for some $c_l > 2$, $G(c_l) \leq -2$. Then according to (3.7) and the fact that $\hat{U}(\eta)$ is increasing, we have that for all $\eta > 0$,

$$\frac{(1-s)c_l - 2}{s} < \hat{U}(\eta) < -2. \tag{3.8}$$

Then we get

$$\frac{(2/c_l-1)\hat{U}(\eta)}{1+1/c_l\hat{U}(\eta)} \geq 2. \tag{3.9}$$

It follows from (3.6a) that

$$\hat{\Theta}'(\eta) \geq 2\frac{\hat{\Theta}(\eta)}{\eta}. \tag{3.10}$$

By direct integration and (3.7), we have that for η large enough,

$$\hat{\Theta}(\eta) \geq C_1\eta^2. \tag{3.11}$$

Using this estimate and (3.7) in (3.6b), we get

$$\hat{W}'(\eta) \geq -\frac{C_2\hat{W}(\eta)}{\eta} + \frac{C_3}{\eta}. \tag{3.12}$$

This implies

$$\left(\eta^{C_2}\hat{W}(\eta)\right)' \geq C_3\eta^{C_2-1}. \tag{3.13}$$

Then we have that for η large enough,

$$\eta^{C_2}\hat{W}(\eta) \geq \frac{C_3}{C_2}\eta^{C_2} - C_4. \tag{3.14}$$

Using this lower bound in (3.6c), we get

$$\hat{U}'(\eta) \geq \frac{C_5}{\eta} - \frac{C_6}{\eta^{C_2+1}}. \tag{3.15}$$

The constants C in the above estimates are positive and independent of η. The inequality (3.15) implies that $\hat{U}(\eta) \to +\infty$ as $\eta \to +\infty$, which contradicts with $G(c_l) \leq -2$. This completes the proof of Lemma 3.1. □

We add a subscript c_l to indicate the dependence of the profiles on c_l for the rest part of this section:

$$\hat{U}_{c_l}(\eta) = \hat{U}(\eta),\ \hat{W}_{c_l}(\eta) = \hat{W}(\eta),\ \hat{\Theta}_{c_l}(\eta) = \hat{\Theta}(\eta). \tag{3.16}$$

Lemma 3.2. *Choose $\Theta_s = 1$ in constructing the power series (2.1), and extend the local profiles to $\mathbf{R}^+$. Then for fixed η, $\hat{U}_{c_l}(\eta)$, $\hat{W}_{c_l}(\eta)$ and $\hat{\Theta}_{c_l}(\eta)$ are continuous functions of c_l.*

Proof. We only need to prove that for fixed $c_l^0 > 2$, $\hat{U}_{c_l}(\eta)$, $\hat{\Theta}_{c_l}(\eta)$ and $\hat{W}_{c_l}(\eta)$ as functions of c_l are continuous at $c_l = c_l^0$. In our construction of the power series using (2.9), we can easily see that the coefficients U_k and Θ_k depend continuously on c_l. And based on the condition (2.10), there exist uniform upper bounds of these coefficients

$$|U_k| \leq \frac{u^0 r^k}{k^2}, \quad |\Theta_k| \leq \frac{\theta^0 r^k}{k}, \tag{3.17}$$

for c_l in a neighborhood of c_l^0. This means there exists a fixed ϵ small enough, such that $\hat{W}_{c_l}(\epsilon)$, $\hat{\Theta}_{c_l}(\epsilon)$ and $\hat{U}_{c_l}(\epsilon)$ are continuous at c_l^0. Then we use the continuous dependence of ODE solutions on initial conditions and parameter to complete the proof of this lemma. □

Now we begin to prove Theorem 3.1. We use an iterative method which enables us to get shaper estimates of the profiles after each iteration. We finally attain that $\hat{U}_{c_l}(\eta)$ converges uniformly to $G(c_l)$, with which we can complete the proof of this theorem.

Proof. Consider $c_l^0 > 2$, we will prove that $G(c_l^0) < +\infty$, and $G(c_l)$ is continuous at $c_l = c_l^0$.

According to Lemma 3.1 and Lemma 3.2, there exist η_0 large enough and a neighborhood of c_l^0, $I_0 = (c_1, c_2)$ with $c_1 > 2, c_2 < +\infty$, such that for $c_l \in I_0$ and $\eta > \eta_0$,

$$\hat{U}_{c_l}(\eta) > \hat{U}_{c_l}(\eta_0) > -2 + \epsilon_1. \tag{3.18}$$

Then for $c_l \in I_0$ and $\eta > \eta_0$, there exists $\epsilon_2 > 0$, such that

$$\frac{(2/c_l - 1)\hat{U}_{c_l}(\eta)}{1 + 1/c_l\hat{U}_{c_l}(\eta)} < 2 - \epsilon_2. \tag{3.19}$$

Using this in (3.6a), we have that for $c_l \in I_0$ and $\eta > \eta_0$,

$$\hat{\Theta}'_{c_l}(\eta) \leq \frac{(2 - \epsilon_2)\hat{\Theta}_{c_l}(\eta)}{\eta}. \tag{3.20}$$

Using direct integration and Lemma 3.2, we have that for $c_l \in I_0$, $\eta > \eta_0$,

$$\hat{\Theta}_{c_l}(\eta) \leq C_1\eta^{2-\epsilon_2}. \tag{3.21}$$

Using this upper bound of $\hat{\Theta}(\eta)$ in (3.6b), we have that for $c_l \in I_0$, $\eta > \eta_0$,

$$\hat{W}'_{c_l}(\eta) \leq \left(\frac{-1}{1 + 1/c_l\hat{U}_{c_l}(\eta)}\right)\frac{\hat{W}_{c_l}(\eta)}{\eta} + C_3\eta^{-1-\epsilon_2}. \tag{3.22}$$

The first term in (3.22) is negative according to (3.7) and the second term is integrable for $\eta > \eta_0$. Then using Lemma 3.2, we have that for $c_l \in I_0$, $\eta > \eta_0$,

$$\hat{W}_{c_l}(\eta) < C_4. \tag{3.23}$$

Putting this upper bound in (3.6c) and using Lemma 3.2, we get that for $c_l \in I_0$, $\eta > \eta_0$,

$$\hat{U}_{c_l}(\eta) < C_5 \ln \eta. \tag{3.24}$$

Putting this upper bound of $\hat{U}(\eta)$ back in (3.6b), we have that for $c_l \in I_0$, $\eta > \eta_0$,

$$\hat{W}'_{c_l}(\eta) < -\frac{C_6\hat{W}_{c_l}(\eta)}{\eta \ln \eta} + C_3\eta^{-1-\epsilon_2}, \tag{3.25}$$

which by direct integration gives that for $c_l \in I_0$, $\eta > \eta_0$,

$$\hat{W}_{c_l}(\eta)\exp\Big(\int_{\eta_0}^{\eta}\frac{C_6}{\zeta \ln \zeta}\mathrm{d}\zeta\Big) < C_7. \tag{3.26}$$

Thus we have that for $c_l \in I_0$ and $\eta > \eta_0$,

$$\hat{W}_{c_l}(\eta) < C_8/\ln \eta. \tag{3.27}$$

Using this sharper upper bound of $\hat{W}(\eta)$ in (3.6c), we get that for $c_l \in I_0$, $\eta > \eta_0$,

$$\hat{U}_{c_l}(\eta) < C_9 \ln \ln \eta. \tag{3.28}$$

Again putting this sharper upper bound in (3.6b), we have that for $c_l \in I_0$, $\eta > \eta_0$,

$$\hat{W}'_{c_l}(\eta) < -\frac{C_{10}\hat{W}_{c_l}(\eta)}{\eta \ln \ln \eta} + C_3\eta^{-1-\epsilon_2}. \tag{3.29}$$

By direct integration, we get

$$\hat{W}_{c_l}(\eta)\exp\Big(\int_{\eta_0}^{\eta}\frac{C_{11}}{\zeta \ln \ln \zeta}\mathrm{d}\zeta\Big) < C_{12}. \tag{3.30}$$

Since $\int_{\eta_0}^{\eta} \frac{C_{11}}{\zeta \ln\ln\zeta} \mathrm{d}\zeta > C_{13}(\ln\eta)^{\alpha} - C_{14}$ for some $\alpha \in (0,1)$, we have that for $c_l \in I_0$, $\eta > \eta_0$,

$$\hat{W}_{c_l}(\eta) < C_{15} \exp\big(-C_{13}(\ln\eta)^{\alpha}\big). \tag{3.31}$$

Note that $C_1, C_2, \dots C_{15}$ in the above estimates are all positive constants independent of η. Using the upper bound of $\hat{W}_{c_l}(\eta)$ (3.31) in (3.6c), we conclude that $\hat{U}_{c_l}(\eta)$ converges uniformly as $\eta \to +\infty$ for $c_l \in I_0$ and complete the proof of this theorem. □

To complete the proof of our main result Theorem 1.1, we still need to verify condition (3.2) for different s. And we leave this part to section 4.

4. Existence of Self-Similar Profiles

In this section, we verify condition (3.2) for $s = 2$, i.e., there exist $c_l^l, c_l^r > 2$, such that $G(c_l^l) < 0$, $G(c_l^r) > 0$, with which we can complete the first half of Theorem 1.1. The following lemma allows us to prove (3.2) using estimates of the profiles at some finite η_0.

Lemma 4.1. *Consider solving equations* (3.6) *with initial conditions given by power series* (2.1). *For some* $\eta_0 > 0$, *let* $u_0 = \hat{U}(\eta_0)$, $\theta_0 = \hat{\Theta}(\eta_0)$, $w_0 = \hat{W}(\eta_0)$.
If

$$u_0 > 0, \tag{4.1a}$$

then

$$G(c_l) > 0. \tag{4.1b}$$

If

$$u_0 > -2, \quad u_0 + c_l w_0 + \frac{(c_l - 2)\theta_0}{(u_0+2)(1+u_0/c_l)\eta_0^2} < 0, \tag{4.1c}$$

then

$$G(c_l) < 0. \tag{4.1d}$$

Proof. $G(c_l) = \lim_{\eta\to+\infty} \hat{U}(\eta)$, and $\hat{U}(\eta)$ is increasing according to (3.6c) and (2.18). So if $u_0 > 0$, then $G(c_l) > u_0 > 0$, and we finish the first part of the Lemma (4.1b).

We prove the second part (4.1d) by contradiction. If $G(c_l) \geq 0$, then there exists $\eta_1 \in (\eta_0, +\infty]$ such that $\hat{U}(\eta_1) = 0$, and for $\eta \in (\eta_0, \eta_1)$, $\hat{U}(\eta) > u_0$. According to (3.6a) we have,

$$\hat{\Theta}'(\eta) \leq \frac{(2/c_l - 1)u_0}{1 + u_0/c_l} \frac{\hat{\Theta}(\eta)}{\eta}. \tag{4.2a}$$

By direct integration, we get that for $\eta \in (\eta_0, \eta_1)$,

$$\hat{\Theta}(\eta) \leq \theta_0 \eta_0^{\frac{(1-2/c_l)u_0}{1+u_0/c_l}} \eta^{\frac{(2/c_l-1)u_0}{1+u_0/c_l}}. \tag{4.2b}$$

Using this upper bound of $\hat{\Theta}$ and the fact that $\hat{U}(\eta) < 0$ for $\eta \in (\eta_0, \eta_1)$ in (3.6b), we get

$$(\hat{W}(\eta)\eta)' \leq \frac{1 - 2/c_l}{(1+u_0/c_l)^2} \theta_0 \eta_0^{\frac{(1-2/c_l)u_0}{1+u_0/c_l}} \eta^{\frac{-u_0-2}{1+u_0/c_l}}. \tag{4.3a}$$

Since $u_0 > -2$, integrating (4.3a) from η_0 to η, we have that for $\eta \in (\eta_0, \eta_1)$,

$$\hat{W}(\eta)\eta \leq w_0\eta_0 + \frac{2/c_l - 1}{(1+u_0/c_l)(u_0/c_l - u_0 - 1)} \theta_0 (\eta_0^{-1} - \eta_0^{\frac{(1-2/c_l)u_0}{1+u_0/c_l}} \eta^{\frac{-u_0-1+u_0/c_l}{1+u_0/c_l}}). \tag{4.3b}$$

Putting this upper bound of $\hat{W}(\eta)$ in (3.6c) and integrating it from η_0 to η_1, we get

$$0 - u_0 = \hat{U}(\eta_1) - \hat{U}(\eta_0) \le c_l w_0 + \frac{(c_l - 2)\theta_0}{(u_0 + 2)(1 + u_0/c_l)\eta_0^2}, \tag{4.4}$$

which contradicts (4.1c). Then we complete the proof of this lemma. □

We use numerical computation with rigorous error control to verify condition (4.1a) or (4.1c). Computer programs have been used to prove mathematical theorems including, to name a few, the four color theorem [1], Kepler conjecture [14] and some others [19, 16, 10]. One method of computer-assisted proof is to use the interval arithmetic and inclusion principle to ensure that the output of a numerical program encloses the solution of the original problem. One first reduces the computation to a sequence of the four elementary operations, and then proceeds by replacing numbers with intervals and performing elementary operations between such intervals of representable numbers under appropriate rounding rules.

To be precise, assume that $x \in [x_{\min}, x_{\max}]$, $y \in [y_{\min}, y_{\max}]$, where $x_{\min}$, $x_{\min}$, $y_{\min}$ and $y_{\max}$ are floating point numbers that can be represented exactly on a computer. Then for one of the four elementary operations, $\odot \in \{+, -, *, /\}$, we have

$$x \odot y \in [z_{\min}, z_{\max}], \tag{4.5a}$$

where

$$z_{\min} = \min\{x_{\min} \underline{\odot} y_{\min}, x_{\min} \underline{\odot} y_{\max}, x_{\max} \underline{\odot} y_{\min}, x_{\max} \underline{\odot} y_{\max}\}, \tag{4.5b}$$

$$z_{\max} = \max\{x_{\min} \overline{\odot} y_{\min}, x_{\min} \overline{\odot} y_{\max}, x_{\max} \overline{\odot} y_{\min}, x_{\max} \overline{\odot} y_{\max}\}, \tag{4.5c}$$

and $\underline{\odot}$ and $\overline{\odot}$ refer to standard floating point operations with rounding modes set to 'DOWNWARD' and 'UPWARD' respectively [23]. Namely, $x \underline{\odot} y$ is the largest floating number less than $x \odot y$, and $x \overline{\odot} y$ is the smallest floating number larger than $x \odot y$. For the case that $\odot$ is division we require that $0 \notin [y_{\min}, y_{\max}]$. The RHS of (4.5) involve only floating point operation, so (4.5) allows us to track the numerical errors using computer programs.

Using the above interval arithmetic strategy, we first numerically construct the power series (2.1) locally with $\Theta_s = 1$, and then extend them to some η_0 by solving the ODE system (3.6) to verify condition (4.1a) or (4.1c). We only illustrate this computer assisted proof procedure for the case $s = 2$ with $c_l^l = 3, c_l^r = 8$. But the same process can be applied to other $s > 2$ to verify the existence of self-similar profiles. The computer programs used for this part of proof can be found at `https://sites.google.com/site/pengfeiliuc/home/codes`.

4.1. **The case $s = 2$, $c_l = 3$.** We verify that for $s = 2$, $G(3) < 0$.

Step 1 We need to control the numerical error in the local power series solutions. To numerically compute (2.1), we first truncate the power series to finite terms. For the case $s = 2$, $c_l = 3$, the following choice of θ^0, u^0 and r makes (2.10) hold:

$$u^0 = \frac{1}{9 \times 162}, \quad \theta^0 = \frac{1}{9 \times 9 \times 162}, \quad r = 162. \tag{4.6}$$

Based on (3.4), at $\xi = 10^{-3}$, corresponding to $\eta_s = 10^{-1}$, we have

$$\hat{U}(\eta_s) = \sum_{k=1}^{\infty} U_k \eta_s^{3k-3}, \quad \hat{\Theta}(\eta_s) = \sum_{k=2}^{\infty} \Theta_k \eta_s^{3k-1}, \quad \hat{W}(\eta_s) = \sum_{k=1}^{\infty} W_k \eta_s^{3k}. \tag{4.7}$$

Using estimates (2.13), if we truncate the power series (4.7) to $m = 20$ terms, the truncation errors of the three series can be bounded respectively by

$$\frac{u^0 r^{m+1}\eta_s^{3m}}{(m+1)^2(1-r\eta_s^3)}, \quad \frac{\theta^0(r\eta_s^3)^{m+1}}{(m+1)(1-r\eta_s^3)\eta_s}, \quad \frac{u^0 r^{m+2}\eta_s^{3m+2}}{(m+2)(1-r\eta_s^3)}. \tag{4.8}$$

Then we need to estimate the truncated power series

$$\hat{U}(\eta_s) \approx \sum_{k=1}^{20} U_k \eta_s^{3k-3}, \quad \hat{\Theta}(\eta_s) \approx \sum_{k=2}^{20} \Theta_k \eta_s^{3k-1}, \quad \hat{W}(\eta_s) \approx \sum_{k=1}^{20} W_k \eta_s^{3k}. \tag{4.9}$$

Using the interval arithmetic (4.5) strategy in each elementary operation of (2.9), we can inductively get computer-representable intervals enclosing the values of U_k and Θ_k for all $k \le 21$. Then we use these intervals in computing (4.9) to get intervals enclosing the values of the truncated power series (4.9). Finally we add back the the intervals (4.8) enclosing the truncation errors using interval arithmetic, and get intervals strictly enclosing $\hat{U}(\eta_s)$, $\hat{W}(\eta_s)$ and $\hat{\Theta}(\eta_s)$. We denote them as

$$I^0_{\hat{U}}, \quad I^0_{\hat{W}}, \quad I^0_{\hat{\Theta}}, \tag{4.10}$$

and use them as initial conditions to solve (3.6).

We use the forward Euler scheme [20] to numerically integrate the ODE system (3.6). For a general ODE system with given initial conditions,

$$y = (y_1(x), y_2(x), \dots y_N(x))^T, \quad y'(x) = f(x,y), \quad x \in [a,b], \quad y(a) = y_0, \tag{4.11}$$

the forward Euler scheme discretizes the domain to finite points, $a = x_0 < x_1 \cdots < x_m = b$ with step size $x_i - x_{i-1} = h$, and the numerical solutions $y_n \approx y(x_n)$ are obtained by

$$y_{n+1} = y_n + hf(x_n, y_n). \tag{4.12}$$

For the solution of the ODE system (4.11), using Taylor expansion, we have

$$y(x_{n+1}) = y(x_n) + hf(x_n, y(x_n)) + 1/2\,(y_1''(x_1^*), y_2''(x_2^*), \dots y_N''(x_N^*))^T\, h^2, \tag{4.13}$$

where $x_i^* \in [x_n, x_{n+1}]$, for $i = 1, 2, \dots N$. Then we have

$$y(x_{n+1}) = y_{n+1} + I_1 + I_2, \tag{4.14}$$

where

$$I_1 = \nabla_y f(x_n, y^*)(y(x_n) - y_n)h, \tag{4.15}$$

$$I_2 = 1/2\,(y_1''(x_1^*), y_2''(x_2^*), \dots y_N''(x_N^*))^T\, h^2, \tag{4.16}$$

and y^* lies between y_n and $y(x_n)$. Note that I_1 is the propagation of error from the previous steps and I_2 is the local truncation error of the integration scheme.

We solve (3.6) from $\eta_s = 10^{-1}$ to $\eta_0 = 3$ with step size $h = 2.9 \times 10^{-6}$, and denote the node point and solutions at the n-th step as

$$\eta^n = 0.1 + nh, \quad (\hat{U}^n, \hat{W}^n, \hat{\Theta}^n)^T, \quad n = 0, \dots, 10^6. \tag{4.17}$$

We already have $I^0_{\hat{U}}$, $I^0_{\hat{W}}$, $I^0_{\hat{\Theta}}$ (4.10) that enclose $\hat{U}^0$, $\hat{W}^0$, $\hat{\Theta}^0$. And we will update

$$I^n_{\hat{U}}, \quad I^n_{\hat{W}}, \quad I^n_{\hat{\Theta}} \tag{4.18}$$

step by step and make sure that they enclose $\hat{U}^n$, $\hat{W}^n$, $\hat{\Theta}^n$.

Step 2 We need to control the roundoff error in computing y_{n+1} (4.12). In the n-th step, we have intervals $I^n_{\hat{U}}$, $I^n_{\hat{W}}$ and $I^n_{\hat{\Theta}}$ that enclose the values of the profiles at η^n. To update these

intervals, we first choose the middle points of these intervals, and use them as the numerical solution y_n. Then we use interval arithmetic to update (4.12) to get intervals enclosing the numerical solutions y_{n+1} at the $n+1$-th step.

Step 3 We need to control the propagation of error from previous steps, I_1. Note that the values of the profiles at η^n are enclosed in intervals $I^n_{\hat{U}}$, $I^n_{\hat{W}}$, $I^n_{\hat{\Theta}}$, and we have used their middle points as the numerical solution y_n. So we use interval arithmetic to deduct the middle points from these intervals and get intervals enclosing $y(x_n) - y_n$ in (4.15). Then we need estimates of the Jacobian matrix of right hand side of (3.6), which is

$$\frac{\partial\left(\hat{W}'(\eta),\hat{U}'(\eta),\hat{\Theta}'(\eta)\right)}{\partial(\hat{W},\hat{U},\hat{\Theta})} = \begin{pmatrix} \frac{-c_l}{c_l\eta+\hat{U}\eta} & \frac{c_l(4\hat{\Theta}-2c_l\hat{\Theta}+(c_l+\hat{U})\eta^2\hat{W})}{(\hat{U}+c_l)^3\eta^3} & \frac{c_l(c_l-2)}{(c_l+\hat{U})^2\eta^3} \\ \frac{c_l}{\eta} & 0 & 0 \\ 0 & \frac{c_l(2-c_l)\hat{\Theta}}{(c_l+\hat{U})^2\eta} & \frac{(2-c_l)\hat{U}}{c_l\eta+\hat{U}\eta} \end{pmatrix} \tag{4.19}$$

Using intervals $I^n_{\hat{U}}, I^n_{\hat{W}}, I^n_{\hat{\Theta}}$ and interval arithmetic in computing (4.19), we can get intervals enclosing each entry of $\nabla_y f(x,y^*)$ in (4.15). Then using interval arithmetic in the matrix-vector multiplication $\nabla_y f(x,y^*)\,(y(x_n)-y_n)$ gives us intervals enclosing I_1.

Step 4 We need to control the local truncation errors I_2 of the scheme, which are

$$\frac{1}{2}\hat{U}''(\eta_1)h^2, \quad \frac{1}{2}\hat{W}''(\eta_2)h^2, \quad \frac{1}{2}\hat{\Theta}''(\eta_3)h^2, \tag{4.20}$$

with $\eta_1,\eta_2,\eta_3 \in [\eta^n,\eta^{n+1}]$. According to (3.6), for $c_l = 3$ we have

$$\hat{W}''(\eta) = \frac{3\eta^2(3+\hat{U}(\eta))\hat{W}(\eta)(6+\hat{U}(\eta)+3\hat{W}(\eta)) - 6\hat{\Theta}(\eta)(6+2\hat{U}(\eta)+3\hat{W}(\eta))}{\eta^4(3+\hat{U}(\eta))^3}, \tag{4.21a}$$

$$\hat{U}''(\eta) = \frac{9\hat{\Theta}(\eta) - 3\eta^2(3+\hat{U}(\eta))(6+\hat{U}(\eta))\hat{W}(\eta)}{\eta^4(3+\hat{U}(\eta))^2}, \tag{4.21b}$$

$$\hat{\Theta}''(\eta) = \frac{\hat{\Theta}(\eta)\hat{U}(\eta)(3+2\hat{U}(\eta)) - 9\hat{\Theta}(\eta)\hat{W}(\eta)}{\eta^2(3+\hat{U}(\eta))^2}. \tag{4.21c}$$

To control the local truncation error (4.20), we need the following *a priori* estimates.

Lemma 4.2. *Consider the ODE system* (3.6) *with* $c_l > 2$ *and initial conditions given by power series* (2.1). *Assuming that at* $\eta^n > 0$, *the solutions are* $\hat{U}^n$, $\hat{W}^n$, $\hat{\Theta}^n$, *then for* $\eta \in [\eta^n,\eta^{n+1}]$, *we have the following* a priori *estimates,*

$$\hat{\Theta}(\eta) \in [\theta_{\min},\theta_{\max}], \quad \hat{U}(\eta) \in [u_{\min},u_{\max}], \quad \hat{W}(\eta) \in [w_{\min},w_{\max}]. \tag{4.22a}$$

with

$$\theta_{\max} = \hat{\Theta}^n(\eta^{n+1}/\eta^n)^{2-c_l+sc_l}, \qquad \theta_{\min} = \hat{\Theta}^n(\eta^{n+1}/\eta^n)^{2-c_l}, \tag{4.22b}$$

$$u_{\min} = \hat{U}^n, \qquad w_{\max} = \hat{W}^n + \frac{s^2c_l\theta_{\max}h}{(c_l-2)(\eta^n)^3}, \tag{4.22c}$$

$$u_{\max} = \hat{U}^n + w_{\max}h/\eta^n, \qquad w_{\min} = \hat{W}^n - h\frac{c_lw_{\max}}{\eta_0(c_l+u_{\min})}. \tag{4.22d}$$

Proof. According to (3.6a) and the lower bound of $\hat{U}(\eta)$ (3.7), we have

$$\hat{\Theta}'(\eta) \le \frac{\hat{\Theta}(\eta)}{\eta}(sc_l - c_l + 2), \quad \hat{\Theta}'(\eta) \ge \frac{\hat{\Theta}(\eta)}{\eta}(2-c_l). \tag{4.23}$$

By direct integration, we can get $\theta_{\max}$ and $\theta_{\min}$. $\hat{U}(\eta)$ is increasing according to (3.6c), so we get the lower bound $u_{\min}$. Then using the upper bound $\theta_{\max}$ and (3.7) in (3.6b), we get

$$\hat{W}'(\eta) \le \frac{s^2 c_l \theta_{\max}}{(c_l-2)(\eta^n)^3}. \tag{4.24}$$

By direct integration we get the upper bound $w_{\max}$. Putting the upper bound of $\hat{W}(\eta)$ in (3.6c), we get the upper bound of $\hat{U}(\eta)$, $u_{\max}$. Using the upper bound $w_{\max}$ and the lower bound $u_{\min}$ in (3.6b), we have

$$\hat{W}'(\eta) \ge -\frac{c_l w_{\max}}{\eta^n(c_l+u_{\min})}. \tag{4.25}$$

By direct integration we can get the lower bound of $\hat{W}(\eta)$, $w_{\min}$. □

Remark 4.1. *The* a priori *estimates* (4.22) *that we get are relatively sharp for small* h *since they deviate from the values of the profiles only by* $O(h)$.

We first use intervals $I^n_{\hat{U}}$, $I^n_{\hat{W}}$ and $I^n_{\hat{\Theta}}$ and the interval arithmetic in (4.22) to get intervals enclosing the values of the profiles in $[\eta^n, \eta^{n+1}]$. Then we can use these intervals and interval arithmetic in (4.21a) to get an interval enclosing the local truncation error (4.20), I_2.

Step 5 Finally, adding up the intervals enclosing the numerical solutions y_{n+1} (Step 2), the intervals enclosing the propagation of errors from previous steps I_1 (Step 3), and the intervals enclosing the local truncation error I_2 (Step 4), we get intervals enclosing the values of the profiles at η^{n+1}, $I^{n+1}_{\hat{W}}$, $I^{n+1}_{\hat{U}}$, I^{n+1}_{Θ}. We keep updating these intervals, and finally get intervals enclosing the values of the self-similar profiles at $\eta = 3$. They are

$$\begin{aligned}
\hat{U}(3) &\in [-1.61167791024607, -1.61167791022341],\\
\hat{W}(3) &\in [0.110808868817194, 1.10808868851010],\\
\hat{\Theta}(3) &\in [0.934100399788941, 9.34100399819680],
\end{aligned}$$

from which (4.1c) follows immediately, and we complete the proof that $G(3) < 0$.

Remark 4.2. *Since* $\hat{W}^n$, $\hat{U}^n$ *and* $\hat{\Theta}^n$ *are enclosed in the intervals* $I^n_{\hat{W}}$, $I^n_{\hat{U}}$ *and* $I^n_{\hat{\Theta}}$, *we can directly use interval arithmetic in* (4.12) *to get intervals enclosing* $y(x_n)+hf(x_n, y(x_n))$. *This strategy avoids estimating the Jacobian matrix* $\nabla_y f(x, y)$, *but will amplify the propagation of errors from previous steps and lead to meaningless numerical results for this problem.*

4.2. **The case** $s = 2$, c_l**=8.** We verify that for $s = 2$, $G(8) > 0$.

The verification of $G(8) > 0$ can be done in the same way. In the construction of the local solutions (2.1), we can easily verify that the choice of

$$u^0 = \frac{1}{6}, \quad \Theta^0 = \frac{1}{18}, \quad r = 6, \tag{4.26}$$

makes the constraint (2.10) hold. Then we truncate the power series (2.1) to the first 20 terms and evaluate them at $\eta_s = 0.7$. Using the same technique as the case $c_l = 3$, we can get intervals enclosing the self-similar profiles at $\eta_s = 0.7$ and denote them as

$$I^0_{\hat{W}}, \quad I^0_{\hat{U}}, \quad I^0_{\hat{\Theta}}. \tag{4.27}$$

Then we begin to numerically solve (3.6) using (4.27). We use the same techniques as the previous case to control the numerical errors introduced in each step of the numerical

integration, and finally get intervals enclosing the profiles at $\eta = 3$. They are

$$\hat{U}(3) \in [5.66176313743309, 5.66176313745025],$$
$$\hat{W}(3) \in [1.13763978495371, 1.13763978496956],$$
$$\hat{\Theta}(3) \in [2.54776073991655, 2.54776074039048],$$

from which (4.1a) follows and we complete the proof that for $s = 2$, $G(8) > 0$.

With $G(3) < 0$, $G(8) > 0$, we conclude that there exists a c_l such that the self-similar equations (1.6) have analytic solutions with the leading order of $\Theta(\xi)$ at $\xi = 0$ being $s = 2$.

Remark 4.3. *We only verify the existence of self-similar profiles for $s = 2$. But the same procedure can be applied to the cases $s > 2$ without difficulty.*

5. Behavior of the Self-Similar Profiles at Infinity

In this section, we prove that the constructed self-similar profiles satisfy the matching condition (1.7b), and that the profiles are analytic with respect to a transformed variable $\zeta = \xi^{-1/c_l}$ at $\zeta = 0$. With this we can complete the proof of Theorem 1.1. This far-field property of the self-similar profiles can explain the Hölder continuity of the velocity field at the singularity time that is observed in numerical simulation of this model.

Theorem 5.1. *For some $c_l > 2$ and $s \geq 2$, if the self-similar profiles constructed using power series* (2.1) *and extended to the whole R^+ satisfy the decay condition* (1.10)*, then the profiles satisfy the matching condition* (1.7b)*. After the following change of variables,*

$$\zeta = \xi^{-1/c_l}, \quad \tilde{U}(\zeta) = U(\xi)\xi^{-1+1/c_l}, \quad \tilde{\Theta}(\zeta) = \Theta(\xi)\xi^{-1+2/c_l}, \quad \tilde{W}(\zeta) = W(\xi)\xi^{1/c_l}, \tag{5.1}$$

$\tilde{U}(\zeta)$, $\tilde{W}(\zeta)$ and $\tilde{\Theta}(\zeta)$ are analytic functions at $\zeta = 0$.

Our strategy is the following: we first prove that $\tilde{U}(\zeta)$, $\tilde{W}(\zeta)$ and $\tilde{\Theta}(\zeta)$ are smooth at $[0, +\infty)$. Then we show that there exist analytic solutions to the ODE system of $\tilde{U}(\zeta)$, $\tilde{W}(\zeta)$, $\tilde{\Theta}(\zeta)$ with the same initial conditions at $\zeta = 0$. Finally we show that smooth solutions to the ODE of $\tilde{U}$, $\tilde{W}$, $\tilde{\Theta}$ with the given initial conditions are unique to complete the proof.

Proof. If the decay condition (1.10) holds, then $\hat{U}(\eta)$ tends to 0 in equation (3.6), so there exists $\eta_0 > 0$ such that for $\eta > \eta_0$,

$$\frac{(2/c_l - 1)\hat{U}(\eta)}{1 + 1/c_l\hat{U}(\eta)} \in (0, 1/2). \tag{5.2}$$

Then based on (3.6a), we have that for $\eta > \eta_0$,

$$\hat{\Theta}'(\eta) \leq \frac{1/2\hat{\Theta}(\eta)}{\eta}, \tag{5.3}$$

which implies that for $\eta > \eta_0$,

$$\hat{\Theta}(\eta) \leq C_1\eta^{1/2}. \tag{5.4}$$

Using this estimate in (3.6b), we have that for $\eta > \eta_0$,

$$\big(\hat{W}(\eta)\eta\big)' \leq C_2\eta^{-3/2}, \tag{5.5}$$

which gives

$$\hat{W}(\eta)\eta < C_3. \tag{5.6}$$

Using the above estimate in (3.6c), we get that for $\eta > \eta_0$,

$$\hat{U}'(\eta) \le C_4 \eta^{-2}, \tag{5.7}$$

which together with $\hat{U}(+\infty) = 0$ implies that for $\eta > \eta_0$,

$$\hat{U}(\eta) \ge -C_5 \eta^{-1}. \tag{5.8}$$

Based on (3.6b) and (3.6c), we have

$$\hat{\Theta}'(\eta) = \frac{(2/c_l - 2)\hat{\Theta}(\eta)\hat{U}(\eta)}{\eta + 1/c_l \hat{U}(\eta)\eta}, \quad (\hat{W}(\eta)\eta)' = \frac{1/c_l \hat{U}(\eta)\hat{W}(\eta)}{1 + 1/c_l \hat{U}(\eta)} + \frac{(1 - 2/c_l)\hat{\Theta}(\eta)}{(1 + 1/c_l \hat{U}(\eta))^2 \eta^2}. \tag{5.9}$$

Using (5.8), (5.6) and (5.4) in (5.9), we can see that $|\hat{\Theta}'(\eta)|$ and $|(\hat{W}(\eta)\eta)'|$ are both integrable from η_0 to $+\infty$, thus $\hat{\Theta}(\eta)$ and $\hat{W}(\eta)\eta$ converge as $\eta \to +\infty$,

$$\lim_{\eta \to \infty} \hat{W}(\eta)\eta = \hat{W}_\infty \in [0, +\infty), \quad \lim_{\eta \to \infty} \hat{\Theta}(\eta) = \hat{\Theta}_\infty \in (0, +\infty). \tag{5.10}$$

Based on (3.6c) and the fact that $\hat{U}(+\infty) = 0$, we have

$$\lim_{\eta \to +\infty} \hat{U}(\eta)\eta = -c_l \hat{W}_\infty. \tag{5.11}$$

The above limits imply that after changing variables, $\tilde{U}(\zeta)$, $\tilde{\Theta}(\zeta)$ and $\tilde{W}(\zeta)$ are continuous for $\zeta \in [0, +\infty)$. The ODE system they satisfy for $\zeta \in (0, +\infty)$ is

$$\tilde{\Theta}'(\zeta) = \frac{(2/c_l - 1)\tilde{\Theta}(\zeta)\tilde{U}(\zeta)}{-1 - \tilde{U}(\zeta)\zeta}, \tag{5.12a}$$

$$\tilde{W}'(\zeta) = \frac{1/c_l \tilde{U}(\zeta)\tilde{W}(\zeta) + (1 - 2/c_l)\tilde{\Theta}(\zeta) - 1/c_l \tilde{\Theta}'(\zeta)\zeta}{-1 - \tilde{U}(\zeta)\zeta}, \tag{5.12b}$$

$$\tilde{U}'(\zeta) = -\frac{\tilde{U}(\zeta)}{\zeta} - \frac{c_l \tilde{W}(\zeta)}{\zeta}, \tag{5.12c}$$

with initial conditions given by (5.10) and (5.11),

$$\tilde{W}(0) = \hat{W}_\infty, \quad \tilde{\Theta}(0) = \hat{\Theta}_\infty, \quad \tilde{U}(0) = -c_l \hat{W}_\infty. \tag{5.12d}$$

Equation (5.12c) can be written as

$$\tilde{U}(\zeta) = -\frac{c_l}{\zeta} \int_0^\zeta \tilde{W}(\eta) \mathrm{d}\eta. \tag{5.13}$$

Using a simple bootstrap argument, we can get $\tilde{W}(\zeta)$, $\tilde{\Theta}(\zeta)$ and $\tilde{U}(\zeta)$ are in $C^\infty\big([0, +\infty)\big)$. On the other hand, given the initial conditions (5.12d), we can construct the following power series solutions to equations (5.12):

$$\tilde{U}(\zeta) = -c_l \hat{W}_\infty + \sum_{k=1}^\infty \tilde{U}_k \zeta^k, \quad \tilde{W}(\zeta) = \hat{W}_\infty + \sum_{k=1}^\infty \tilde{W}_k \zeta^k, \quad \tilde{\Theta}(\zeta) = \hat{\Theta}_\infty + \sum_{k=1}^\infty \tilde{\Theta}_k \zeta^k. \tag{5.14}$$

Plugging these power series ansatz in (5.12) and matching the coefficients of ζ^k, we can uniquely determine the coefficients $\tilde{U}_k$, $\tilde{W}_k$, $\tilde{\Theta}_k$ and prove that the power series (5.14) converge in a small neighborhood of $\zeta = 0$. We omit the details here, because the argument is the same as section 2. Then to prove the analyticity of $\tilde{U}(\zeta)$, $\tilde{W}(\zeta)$ and $\tilde{\Theta}(\zeta)$ at $\zeta = 0$, we only need the uniqueness of smooth solutions to (5.12) with initial condition (5.12d). The RHS of (5.12c) is not Lipschitz, so the classical uniqueness result will not apply here.

Assume $\tilde{U}^i(\zeta)$, $\tilde{W}^i(\zeta)$, $\tilde{\Theta}^i(\zeta)$, $i = 1, 2$, are two different solutions to equation (5.12) with initial condition (5.12d). And let $\delta U(\zeta)$, $\delta W(\zeta)$, $\delta\Theta(\zeta)$ be the difference of the two solutions,

$$\delta\tilde{U}(\zeta) = \tilde{U}^1(\zeta) - \tilde{U}^2(\zeta), \quad \delta\tilde{W}(\zeta) = \tilde{W}^1(\zeta) - \tilde{W}^2(\zeta), \quad \delta\tilde{\Theta}(\zeta) = \tilde{\Theta}^1(\zeta) - \tilde{\Theta}^2(\zeta). \tag{5.15}$$

Then based on (5.12c),

$$\delta U(\zeta) = -\frac{c_l}{\zeta}\int_0^\zeta \delta W(\zeta)\mathrm{d}\zeta. \tag{5.16}$$

Using Hardy inequality[12], there exists C_1 independent of ϵ such that

$$\|\delta\tilde{U}\|_{L^2([0,\epsilon])} \le C_1\|\delta\tilde{W}\|_{L^2([0,\epsilon])}. \tag{5.17}$$

Since the right hand side of (5.12a) and (5.12b) are Lipschitz continuous, we have

$$|\frac{\mathrm{d}}{\mathrm{d}\zeta}(\delta\tilde{W}(\zeta))| + |\frac{\mathrm{d}}{\mathrm{d}\zeta}(\delta\tilde{\Theta}(\zeta)))| \le C_2(|\delta\tilde{W}(\zeta)| + |\delta\tilde{U}(\zeta)| + |\delta\tilde{\Theta}(\zeta)|) \tag{5.18}$$

Integrating the square of both sides on the interval $[0, \epsilon]$ and using (5.17), we get

$$\|\big(\delta\tilde{W}(\zeta)\big)'\|_{L^2([0,\epsilon])} + \|\big(\delta\tilde{\Theta}(\zeta)\big)'\|_{L^2([0,\epsilon])} \le C_3(\|\delta\tilde{W}(\zeta)\|_{L^2([0,\epsilon])} + \|\delta\tilde{\Theta}(\zeta)\|_{L^2([0,\epsilon])}). \tag{5.19}$$

Since $\delta\tilde{W}(\zeta)$ and $\delta\tilde{\Theta}(\zeta)$ vanish at $\zeta = 0$, by Poincaré-Friedrichs inequality we have

$$\|\delta\tilde{W}(\zeta)\|_{L^2([0,\epsilon])} + \|\delta\tilde{\Theta}(\zeta)\|_{L^2([0,\epsilon])} \le C_4\epsilon(\|\big(\delta\tilde{W}(\zeta)\big)'\|_{L^2([0,\epsilon])} + \|\big(\delta\tilde{\Theta}(\zeta)\big)'\|_{L^2([0,\epsilon])}). \tag{5.20}$$

The C in the above estimates are all positive constants independent of ϵ. Choosing ϵ small enough, we get a contradiction between (5.19) and (5.20), thus

$$\tilde{W}^1 = \tilde{W}^2, \quad \tilde{U}^1 = \tilde{U}^2, \quad \tilde{\Theta}^1 = \tilde{\Theta}^2, \tag{5.21}$$

which means the solution is unique. And we complete the proof of this theorem. □

The above theorem implies that the self-similar profiles that we construct are non-conventional in the sense that the velocity does not decay to 0 at $+\infty$ but grows with certain fractional power. Coming back to the self-similar ansatz (1.4), we have

$$u(x,t) = (T-t)^{c_l-1}U\left(\frac{x}{(T-t)^{c_l}}\right). \tag{5.22}$$

For t close to T, based on Theorem 5.1 , we have

$$u(x,t) \approx C(T-t)^{c_l-1}\frac{x}{(T-t)^{c_l}}\left(\frac{x}{(T-t)^{c_l}}\right)^{-\frac{1}{c_l}} = Cx^{1-\frac{1}{c_l}}. \tag{5.23}$$

This explains the Hölder continuity of the velocity at the singularity time observed in numerical simulation of the 1D model, which was also observed for the 3D Euler equations [15].

6. Numerical Results

In this section we numerically locate the root of $G(c_l)$ for several s and construct the corresponding self-similar profiles. The obtained c_l and self-similar profiles are consistent with numerical simulation of the CKY model. We also find that for fixed leading order of $\theta(x, 0)$, the singular solutions using different initial conditions converge to the same self-similar profiles, which implies that the self-similar profiles have some stability.

6.1. **Numerical methods for solving the self-similar equations.** For any fixed $c_l > 2$, we first numerically compute the coefficients Θ_k, U_k in (2.1) up to $k = 50$ and determine the convergence radius of the power series using the following linear regression for $s \le k \le 50$,

$$\log \Theta_k = k \log r_1 + c_1, \quad \log U_k = k \log r_2 + c_2. \tag{6.1}$$

We choose $r = 1/2 \min\{1/r_1, 1/r_2\}$ and construct the truncated power series (2.1) on $[0, r/2]$.

Then we continue to solve equation (1.9) from $\xi = r/2$ to $\xi = 1$ using the 4th order explicit Runge-Kutta method with step-size $h = \frac{1-r/2}{10^4}$. After $\xi = 1$, we make the change of variables (3.4) and solve (3.6) from $\eta = 1$ to $\eta = 10^5$ using 4th order Runge-Kutta method with step-size $h = \frac{10^5-1}{10^6}$. We use $\hat{U}_{c_l}(10^5)$ as an approximation to $G(c_l)$.

We use the bisection method to find the root of $G(c_l)$. After getting c_l, we construct the local self-similar profiles using power series (2.1) and extend them from $\xi = r/2$ to $\xi = 10$ using the explicit 4th order Runge-Kutta method with step-size $h = \frac{9}{10^4}$. Then we locate the maxima of W, which is $W_{\max} = W(\xi_0)$. For the cases that we consider, $s = 2, 3, 4, 5$, ξ_0 are all less than 10. Finally we rescale the maxima of $W(\xi)$ to $(1, 1)$, and get

$$W_s(\xi) = \frac{1}{W_{\max}} W(\xi\xi_0), \quad \xi \in [0, 1]. \tag{6.2}$$

We only compare the self-similar profiles W_s with direct simulation of the CKY model in this paper, but the numerical results for the profiles Θ and U are similar.

6.2. **Numerical methods for simulating the model.** We use a particle method to simulate the model and consider $N + 1$ particles with position, density and vorticity given by

$$\begin{cases} q = (q_0(t), q_1(t), \dots q_N(t))^T, \\ \theta = (\theta_0(t), \theta_1(t), \dots \theta_N(t))^T, \\ w = (w_0(t), w_1(t), \dots w_N(t))^T. \end{cases} \tag{6.3}$$

In computing the velocity field, we use the trapezoidal rule to approximate (1.6c),

$$u_i = -q_i \left(\sum_{j=i}^{N-1} \frac{w_j + w_{j+1}}{2} (q_{j+1} - q_j) \right). \tag{6.4}$$

In computing the driving force of w, which is θ_x, we use the three points rule:

$$(\theta_x)_i = \begin{cases} 0, & i = 0, \\ \frac{\theta_i - \theta_{i+1}}{q_i - q_{i+1}} + \frac{\theta_i - \theta_{i-1}}{q_i - q_{i-1}} + \frac{\theta_{i+1} - \theta_{i-1}}{q_{i+1} - q_{i-1}}, & 0 < i < N, \\ \frac{\theta_i - \theta_{i-2}}{q_i - q_{i-2}} + \frac{\theta_i - \theta_{i-1}}{q_i - q_{i-1}} + \frac{\theta_{i-2} - \theta_{i-1}}{q_{i-2} - q_{i-1}}, & i = N. \end{cases} \tag{6.5}$$

Initially, 10^5+1 particles are equally placed in the short interval $[0, 10^{-3}]$, which are sufficient to resolve the solutions in the self-similar regime. Outside this short interval $10^5 - 10^2$ particles are equally placed. So the total number of particles is $N + 1 = 2 \times 10^5 - 10^2$.

Then we need to solve the following ODE system

$$\frac{\mathrm{d}}{\mathrm{d}t} q = u, \quad \frac{\mathrm{d}}{\mathrm{d}t} w = \theta_x, \quad \frac{\mathrm{d}}{\mathrm{d}t} \theta = 0. \tag{6.6}$$

The initial condition of θ is

$$\theta(x, 0) = (1 - \cos(\pi x))^{s/2}, \tag{6.7}$$

whose leading order at $x = 0$ is s.

We solve the ODE system (6.6) using the 4-th order explicit Runge-Kutta method, and the time step dt is chosen adaptively to avoid the particles crossing each other:

$$dt_i = \frac{1}{\max(\frac{u_i - u_{i+1}}{q_{i+1}-q_i}, 0)}, \quad dt = \min(\frac{dt_i}{10}, 10^{-3}). \tag{6.8}$$

At each time step, we record the maximal vorticity $w_{\max}(t_i)$, and the position where it is attained $q_{\max}(t_i)$. According to the self-similar ansatz (1.4), we have

$$w_{\max}(t) = C_1(T-t)^{c_w}, \quad q_{\max}(t) = C_2(T-t)^{c_l}. \tag{6.9}$$

Thus we can compute c_l, c_w, and the singularity time T through linear regressions,

$$\left(\frac{\mathrm{d}}{\mathrm{d}t}\log w_{\max}(t)\right)^{-1} \approx -\frac{1}{c_w}t + \frac{T}{c_w}, \tag{6.10a}$$

$$\left(\frac{\mathrm{d}}{\mathrm{d}t}\log q_{\max}(t)\right)^{-1} \approx -\frac{1}{c_l}t + \frac{T}{c_l}. \tag{6.10b}$$

We compute the time derivatives of $\log w_{\max}(t)$ and $\log q_{\max}(t)$ using the center difference method, and the linear regressions (6.10) are done in some time interval close to the singularity time while the numerical solutions still have good accuracy.

At certain time steps close to the singularity time, t^i, $i = 1, 2, 3$, let w^i be the maximal vorticity at time t^i and q^i be the position the maximal vorticity is attained. We rescale the numerical solution and get the self-similar profiles of w,

$$W_s^i(\xi) = \frac{1}{w_{\max}} w(\xi q^i, t^i), \quad \xi \in [0, 1]. \tag{6.11}$$

We will compare the self-similar profiles $W_s^i(\xi)$ (6.11) obtained from direct simulation of the model, with $W_s(\xi)$ (6.2) obtained from solving the self-similar equations (1.6).

Near the singularity time the velocity field seems to be Hölder continuous near the origin,

$$u(x, T) \approx Cx^\alpha. \tag{6.12}$$

Then we can determine the Hölder exponent α through linear regression

$$\ln u(x, T) \approx \ln C + \alpha \ln x. \tag{6.13}$$

We will compare the exponents α (6.13) obtained from the singular solutions, with $1 - 1/c_l$ (5.23) obtained from analyzing the self-similar equations (1.6).

6.3. **Comparison results.** In simulating the CKY model, we first choose $w(x, 0)$ as

$$w(x, 0) = 1 - \cos(4\pi x). \tag{6.14}$$

We compute the scaling exponents c_w and c_l for different leading orders of θ, $s = 2, 3, 4, 5$ using (6.10a) and (6.10b), and the results are listed in Table 1 and Table 2. The Hölder exponents of the velocity field at the singularity time (6.13) and $1 - 1/c_l$ are listed in Table 3. The c_l we use are obtained from solving the self-similar equations.

For $s = 2$, the linear regressions (6.10a) and (6.10b) are done in the time interval

$$[6.4371 \times 10^{-1}, 6.4391 \times 10^{-1}], \tag{6.15}$$

and the predicted singularity time T for (6.10a) and (6.10b) are both 6.4402×10^{-1}. The linear regression (6.13) is done at $t = 6.4391 \times 10^{-1}$ and on the interval $[10^{-10}, 10^{-9}]$.

	$s=2$	$s=3$	$s=4$	$s=5$
c_w	-0.9747	-1.0001	-1.0006	-1.0007

TABLE 1. c_w table

For $s=3$, the linear regressions (6.10a) and (6.10b) are done in the time interval

$$[6.804297\times10^{-1}, 6.804300\times10^{-1}], \tag{6.16}$$

and the predicted singularity time T for (6.10a) and (6.10b) are both 6.804302×10^{-1}. The linear regression (6.13) is done at $t=6.804302\times10^{-1}$ and on the interval $[10^{-10}, 10^{-9}]$.

For $s=4$, the linear regressions (6.10a) and (6.10b) are done in the time interval

$$[6.571218\times10^{-1}, 6.571221\times10^{-1}], \tag{6.17}$$

and the predicted singularity time T for (6.10a) and (6.10b) are both 6.571223×10^{-1}. The linear regression (6.13) is done at $t=6.571223\times10^{-1}$ and on the interval $[10^{-10}, 10^{-9}]$.

For $s=5$, the linear regressions (6.10a) and (6.10b) are done in the time interval

$$[5.9698511\times10^{-1}, 5.9698515\times10^{-1}], \tag{6.18}$$

and the predicted singularity time T for (6.10a) and (6.10b) are both 5.9698517×10^{-1}. The linear regression (6.13) is done at $t=5.9698517\times10^{-1}$ and on the interval $[10^{-10}, 10^{-9}]$.

From the Table 1, 2, 3, we can see that the exponents c_w we obtain from the singular numerical solutions are close to -1 (1.5). And the c_l we obtain from the singular solution (6.10b) are close to those obtained from solving the self-similar equations. At the singularity time, the Hölder exponents of the velocity field are close to $1-1/c_l$.

For the case $s=2$, the dependence of $G(c_l)$ on c_l is plotted in Figure 1. We can see that $G(c_l)$ seems to be a monotone increasing function, which implies that for fixed s, the scaling exponent c_l to make the decay condition (1.10) hold is unique.

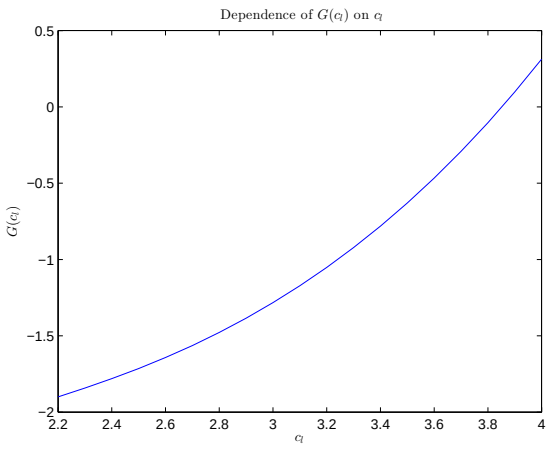

FIGURE 1. Dependence of $G(c_l)$ on c_l for $s=2$

The self-similar profiles that are obtained from solving the self-similar equation (6.2) and from direct simulation of the model (6.11) are plotted in Figure 2. The lines labeled 'exact' are obtained from solving the self-similar equation (6.2). Others are obtained from rescaling the solution at different time steps corresponding to different maximal vorticity.(6.11)

	$s=2$	$s=3$	$s=4$	$s=5$
Linear Regression	3.7942	3.3143	3.1718	3.0773
Self-Similar Equations	3.7967	3.3157	3.1597	3.0841

TABLE 2. c_l got from linear regression (6.10b) and the self-similar equations (1.6).

	$s=2$	$s=3$	$s=4$	$s=5$
Hölder exponent	7.3381×10^{-1}	6.9823×10^{-1}	6.9131×10^{-1}	6.7610×10^{-1}
$1-1/c_l$	7.3661×10^{-1}	6.9841×10^{-1}	6.8351×10^{-1}	6.7576×10^{-1}

TABLE 3. Hölder exponent of the velocity field at 0 and $1-1/c_l$.

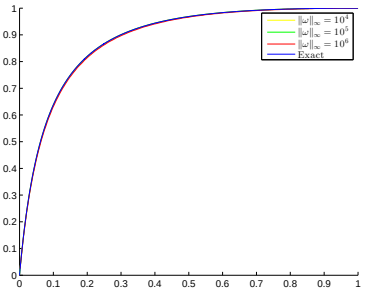

(A) The re-scaled solutions and self-similar profiles we construct. $s=2$.

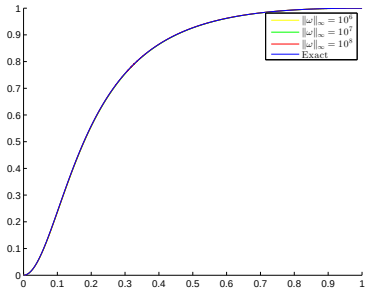

(B) The re-scaled solutions and self-similar profiles we construct. $s=3$.

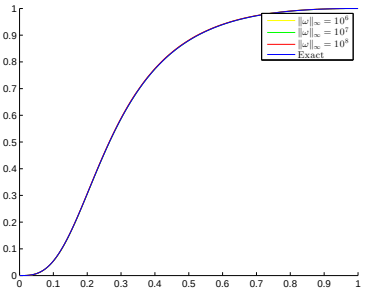

(C) The re-scaled solutions and self-similar profiles we construct. $s=4$.

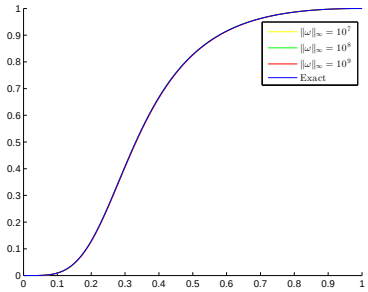

(D) The re-scaled solutions and self-similar profiles we construct. $s=5$.

FIGURE 2. Self-similar profiles of w using initial condition $w(x,0)=1-\cos(4\pi x)$.

To demonstrate the stability the self-similar profiles, we consider another initial condition,

$$w(x,0)=x-x^2. \tag{6.19}$$

The profiles obtained from rescaling the singular solutions (6.11) are plotted in Figure 3.

From Figure 2, 3, we can see that after rescaling, the singular solutions at different time steps before the singularity time are very close, which implies that the solutions develop self-similar singularity. Besides, the self-similar profiles obtained from direct simulation of the model (6.11) agree very well with the self-similar profiles (6.2) we construct by sovling the self-similar equations (1.6). Moreover, for fixed leading order of $\theta(x,0)$ at the origin, the singular solutions with different initial conditions converge to the same set of self-similar profiles, which implies that the profiles have some stability property.

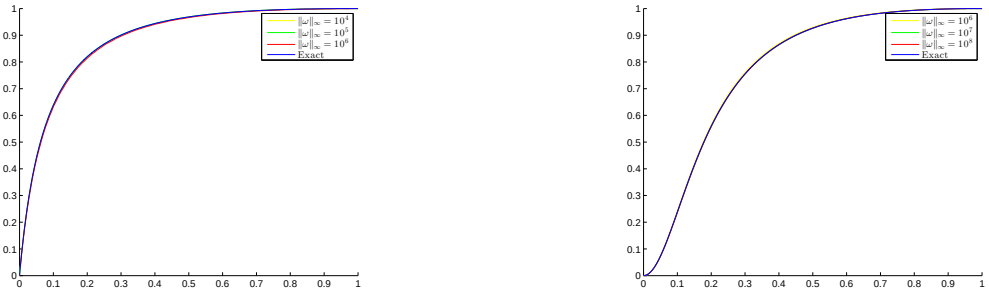

(A) $s = 2$ (B) $s = 3$

FIGURE 3. Self-similar profiles of w using initial condition $w(x, 0) = x - x^2$.

Remark 6.1. *If the initial leading order of $\theta(x, 0)$ is $s \geq 3$, and a small perturbation of θ, which we denote by $\epsilon\tilde{\theta}(x, t)$, has leading order $2 \leq \tilde{s} < s$, then the profiles of the perturbed singular solutions will be determined by $\tilde{s}$, not s. From this point of view, only the self-similar profiles for $s = 2$ are stable in the sense of perturbation.*

7. Concluding Remarks

The existence of a discrete family of analytic self-similar profiles corresponding to different leading orders of the solutions at the origin for the CKY model has been established. The profiles are constructed using a power series method near the origin, and then extended to infinity by solving an ODE system. The decay condition in the Biot-Savart law determines the scaling exponents in the self-similar solutions. Numerical computation together with rigorous error estimation is used to prove the existence of these self-similar profiles. Far-field properties of the self-similar profiles are analyzed. The constructed self-similar profiles are consistent with direct simulation of the model and enjoy some stability property. The current method of analysis does not generalize directly to study the 3D Euler singularity. A new set of techniques are required to deal with the non-local Biot-Savart law. The existence of self-similar singularity for the 3D Euler equations is under investigation.

Acknowledgements. The authors would like to thank Professors Russel Caflisch and Guo Luo for a number of stimulating discussions. We would also like to thank Professors Alexander Kiselev and Yao Yao for their interest in our work and for their valuable comments. The research was in part supported by NSF FRG Grant DMS-1159138.

References

[1] Kenneth Appel and Wolfgang Haken. Proof of 4-color theorem. *Discrete Mathematics*, 16(2):179–180, 1976.
[2] Claude Bardos and Edriss Titi. Euler equations for incompressible ideal fluids. *Russian Mathematical Surveys*, 62(3):409, 2007.
[3] Dongho Chae. Nonexistence of asymptotically self-similar singularities in the euler and the navier–stokes equations. *Mathematische Annalen*, 338(2):435–449, 2007.
[4] Dongho Chae. Nonexistence of self-similar singularities for the 3d incompressible euler equations. *Communications in Mathematical Physics*, 273(1):203–215, 2007.
[5] Dongho Chae. On the self-similar solutions of the 3d euler and the related equations. *Communications in Mathematical Physics*, 305(2):333–349, 2011.

[6] Kyudong Choi, Thomas Y. Hou, Alexander Kiselev, Guo Luo, Vladimir Sverak, and Yao Yao. On the fiinite-time blowup of a 1d model for the 3d axisymmetric euler equations. *arXiv preprint arXiv:1407.4776*, 2014.
[7] Kyudong Choi, Alexander Kiselev, and Yao Yao. Finite time blow up for a 1d model of 2d boussinesq system. *arXiv preprint arXiv:1312.4913*, 2013.
[8] Earl A Coddington and Norman Levinson. *Theory of ordinary differential equations*. Tata McGraw-Hill Education, 1955.
[9] Peter Constantin. On the euler equations of incompressible fluids. *Bulletin of the American Mathematical Society*, 44(4):603–621, 2007.
[10] Charles L Fefferman and Luis A Seco. Interval arithmetic in quantum mechanics. In *Applications of interval computations*, pages 145–167. Springer, 1996.
[11] Gerald B Folland. *Introduction to partial differential equations*. Princeton University Press, 1995.
[12] D.J.H. Garling. *Inequalities: a journey into linear analysis*, volume 19. Cambridge University Press Cambridge, 2007.
[13] John D Gibbon. The three-dimensional euler equations: Where do we stand? *Physica D: Nonlinear Phenomena*, 237(14):1894–1904, 2008.
[14] Thomas C Hales. A proof of the kepler conjecture. *Annals of mathematics*, pages 1065–1185, 2005.
[15] Thomas Y Hou and Guo Luo. On the finite-time blowup of a 1d model for the 3d incompressible euler equations. *arXiv preprint arXiv:1311.2613*, 2013.
[16] R Baker Kearfott and Vladik Kreinovich. *Applications of interval computations*, volume 3. Kluwer Academic Dordrecht, 1996.
[17] Alexander Kiselev and Vladimir Sverak. Small scale creation for solutions of the incompressible two dimensional euler equation. *arXiv preprint arXiv:1310.4799*, 2013.
[18] Sof'ja V Kovalevskaja. Zur theorie der partiellen differentialgleichungen. 1874.
[19] Oscar E Lanford III. A computer-assisted proof of the feigenbaum conjectures. *Bulletin of the American Mathematical Society*, 6(3):427–434, 1982.
[20] Randall J LeVeque. *Finite difference methods for ordinary and partial differential equations: steady-state and time-dependent problems*, volume 98. Siam, 2007.
[21] Guo Luo and Thomas Y Hou. Potentially singular solutions of the 3d incompressible euler equations. *arXiv preprint arXiv:1310.0497*, 2013.
[22] Andrew J Majda and Andrea L Bertozzi. *Vorticity and incompressible flow*, volume 27. Cambridge University Press, 2002.
[23] Dan Zuras, Mike Cowlishaw, Alex Aiken, Matthew Applegate, David Bailey, Steve Bass, Dileep Bhandarkar, Mahesh Bhat, David Bindel, Sylvie Boldo, et al. Ieee standard for floating-point arithmetic. *IEEE Std 754-2008*, pages 1–70, 2008.

SELF-SIMILAR SINGULARITY OF A 1D MODEL FOR THE 3D AXISYMMETRIC EULER EQUATIONS

THOMAS Y. HOU AND PENGFEI LIU

Abstract. We investigate the self-similar singularity of a 1D model for the 3D axisymmetric Euler equations, which is motivated by a particular singularity formation scenario observed in numerical computation. We prove the existence of a discrete family of self-similar profiles for this model and analyze their far-field properties. The self-similar profiles we find agree with direct simulation of the model and seem to have some stability.

1. Introduction and Main Results

Whether the 3D Euler equations develop finite-time singularity is regarded as one of the most important open problems in mathematical fluid mechanics. Interested readers may consult the survey [7] and references therein for more historical background about this outstanding problem. In this paper we investigate the self-similar singularity of a 1D model for the 3D axisymmetric Euler equations, which is motivated by a particular singularity formation scenario observed in numerical computation [10]. It is hoped that this work may help to understand the singularity formation of the 3D Euler equations.

In the numerical computation of Luo and Hou [10], the 3D axisymmetric Euler equations [11] are numerically solved in a periodic cylinder,

$$u_{1,t} + u^r u_{1,r} + u^z u_{1,z} = 2u_1\phi_{1,z}, \tag{1.1a}$$

$$w_{1,t} + u^r w_{1,r} + u^z w_{1,z} = (u_1^2)_z, \tag{1.1b}$$

$$-[\partial_r^2 + (3/r)\partial_r + \partial_z^2]\phi_1 = w_1, \tag{1.1c}$$

where $u^r = -r\phi_{1,z}$, $u^z = 2\phi_1 + r\phi_{1,r}$ are radial and axial velocity, and $u_1 = u^\theta/r$, $w_1 = w^\theta/r$, $\phi_1 = \phi^\theta/r$ are transformed angular velocity, vorticity and stream function respectively.

According to the numerical results reported in [10], the solutions to (1.1) develop self-similar singularity in the meridian plane for certain initial conditions with no flow boundary condition at $r = 1$. The solid boundary and special symmetry of u^θ, ω^θ and ψ^θ along the axial direction seem to make the flow in the meridian plane remain hyperbolic near the singularity point and be responsible for the observed finite-time singularity. A 1D model which approximates the dynamics of the 3D axisymmetric Euler equations along the solid boundary of the periodic cylinder $r = 1$ has been proposed and investigated by Hou and Luo in [8]. The finite-time singularity of this model is proved very recently by Choi, Hou, Kiselev, Luo, Sverak and Yao in [4]. Motivated by this new singularity formation scenario, Kiselev and Sverak [9] construct an example of 2D Euler solutions in a setting similar to [10]. In this example, the gradient of vorticity is proved to exhibit double exponential growth in time, which is known to be the fastest possible rate of growth for the 2D Euler equations. This example provides further evidence that the new singularity formation scenario reported in [10] is an interesting candidate to investigate the 3D Euler singularity.

California Institute of Technology, Applied and Computational Mathematics.

Inspired by the work of [8] and [9], Choi, Kiselev, and Yao proposed the following 1D model (we call it the CKY model for short) [5] on $[0,1]$:

$$\partial_t w + u\partial_x w = \partial_x \rho, \tag{1.2a}$$

$$\partial_t \rho + u\partial_x \rho = 0, \tag{1.2b}$$

$$u(x,t) = -x\int_x^1 \frac{w(y,t)}{y}\mathrm{d}y, \tag{1.2c}$$

$$w(0,t) = 0, \quad \rho(0,t) = 0, \quad \partial_x \rho(0,t) = 0. \tag{1.2d}$$

This 1D model, whose finite-time singularity has been proved in [5], can be viewed as a simplified approximation to the 1D model proposed by Hou and Luo in [8]. Like the 1D model of Hou and Luo, the CKY model approximates the 3D axisymmetric Euler equations (1.1) on the boundary of the cylinder $r = 1$ with

$$\rho \sim u_1^2, \quad w \sim w_1, \quad u \sim u^z. \tag{1.3}$$

The positiveness of $\rho_x(x,t)$ near the origin creates a compressive flow, which is the driving force of the finite-time singularity, and we will use this fact in our construction in section 2. Our numerical simulation suggests that this 1D model develops finite-time singularity in a way similar to that of the 3D axisymmetric Euler equations on the boundary of the cylinder as reported in [10], and the singular solutions to this model also develop self-similar structure. We investigate the self-similar singularity of this CKY model in this paper.

Since the finite-time singularity of the CKY model takes place near the origin, we consider the following self-similar ansatz with ρ, W and U being the self-similar profiles,

$$\rho(x,t) = (T-t)^{c_\rho}\rho\left(\frac{x}{(T-t)^{c_l}}\right), \tag{1.4a}$$

$$u(x,t) = (T-t)^{c_u}U\left(\frac{x}{(T-t)^{c_l}}\right), \tag{1.4b}$$

$$w(x,t) = (T-t)^{c_w}W\left(\frac{x}{(T-t)^{c_l}}\right). \tag{1.4c}$$

Plugging these self-similar ansatz into equations (1.2) and matching the exponents of $(T-t)$ for each equation, we get

$$c_w = -1, \quad c_u = c_l - 1, \quad c_\rho = c_l - 2. \tag{1.5}$$

And the self-similar profiles $U(\xi)$, $W(\xi)$, $\rho(\xi)$ satisfy the following equations defined on $\mathbf{R}^+$,

$$(2-c_l)\rho(\xi) + c_l\xi\rho'(\xi) + U(\xi)\rho'(\xi) = 0, \tag{1.6a}$$

$$W(\xi) + c_l\xi W'(\xi) + U(\xi)W'(\xi) - \rho'(\xi) = 0, \tag{1.6b}$$

$$U(\xi) = -\xi\int_\xi^\infty \frac{W(\eta)}{\eta}\mathrm{d}\eta. \tag{1.6c}$$

We refer equations (1.6) as the self-similar equations, which can be easily verified to enjoy the following scaling-invariant property:

$$U(\xi) \to \frac{1}{\lambda}U(\lambda\xi), \quad W(\xi) \to W(\lambda\xi), \quad \rho(\xi) \to \frac{1}{\lambda}\rho(\lambda\xi). \tag{1.7}$$

In this paper we study the existence and properties of solutions to the self-similar equations. A key fact for the CKY model is that the Biot-Savart law (1.6c) in the self-similar equations can be rewritten as a local relation with a decay condition,

$$\left(\frac{U(\xi)}{\xi}\right)' = \frac{W(\xi)}{\xi}, \tag{1.8a}$$

$$\lim_{\eta\to+\infty} \frac{U(\xi)}{\xi} = 0. \tag{1.8b}$$

We first ignore the decay condition (1.8b), then the self-similar equations with (1.6c) replaced by (1.8a) become a nonlinear ODE system with singular RHS at $\xi = 0$, i.e., the RHS does not satisfy the Lipschitz condition. We construct solutions to this ODE system near $\xi = 0$ using a power series method, which can naturally overcome the singularity of the RHS at $\xi = 0$. The power series are unique up to a rescaling parameter for a fixed leading order of $\rho(\xi)$ at $\xi = 0$, and can be extended to the whole $\mathbf{R}^+$ by solving the ODE system. Then we prove that the decay condition (1.8b) determines the scaling exponents, and there exist a discrete family of c_l, corresponding to different leading orders of $\rho(\xi)$, such that the decay condition (1.8b) holds for the self-similar profiles we construct . We prove this part with the assistance of numerical computation and rigorous error estimation. Given the decay condition (1.8b), we further analyze the far-field behavior of these self-similar profiles and prove that the profiles are analytic with respect to a transformed variable at $\xi = +\infty$.

Our main results include the following two Theorems:

Theorem 1.1. *There exist a discrete family of scaling exponent c_l and solutions to equations (1.6), corresponding to different leading orders of the self-similar profile $\rho(\xi)$ at $\xi = 0$,*

$$s = \min\{k \in N^+| \ \frac{\mathrm{d}^k}{\mathrm{d}\xi^k}\rho(0) \neq 0\}. \tag{1.9}$$

Theorem 1.2. *In the near-field, the self-similar profiles $W(\xi)$, $U(\xi)$, $\rho(\xi)$ we construct are analytic with respect to ξ at $\xi = 0$. And in the far-field, $W(\xi)$, $U(\xi)\xi^{-1}$, $\rho(\xi)\xi^{-1}$ are analytic with respect to a transformed variable $\theta = \xi^{-1/c_l}$ at $\theta = 0$.*

An interesting fact for this 1D model is that self-similar profiles (1.4) exist only for a discrete set of the scaling exponent c_l, corresponding to different leading orders of $\rho(x, t)$ at $x = 0$. The self-similar profiles we find agree with direct simulation of the model and seem to have some stability in the sense that for fixed leading order of $\rho(x, 0)$, the singular solutions using different initial conditions converge to the same set of self-similar profiles.

The self-similar profiles we construct are non-conventional in the sense that the velocity does not decay to 0 at infinity but grows with certain fractional power, correspondingly, the velocity field at the singularity time is Hölder continuous. Such behavior is also observed in the numerical simulation of the 3D Euler equations in [8], which is very different from the Leray type of self-similar solutions of the 3D Euler equations, whose existence has been ruled out under certain decay assumptions on the self-similar profiles [2, 1, 3].

Our method of analysis is of interest by itself. The existence result replies on the use of a power series method to deal with the singularity of the self-similar equations at the origin, and some very subtle and relatively sharp estimates of the self-similar profiles. The same approach can be taken to analyze the self-similar singularity of Burgers equation and get results similar to those obtained in this paper. We are currently investigating the possibility of extending this method to study the singularity of the 2D Boussinesq system.

Another novelty in our analysis is the use of numerical computation with rigorous error control, which is an important step in establishing the existence of self-similar solutions. Our strategy to rigorously control the numerical error, including the numerical error of the integration scheme for an ODE system and the roundoff error introduced due to floating point operation, is quite general and can be used for other purposes.

The rest of this paper is organized as follows. In section 2, we construct the local self-similar profiles using a power series method and extend them to the whole $\mathbf{R}^+$. In section 3, we prove that the decay condition in the Biot-Savart law determines the scaling exponents in the self-similar solutions. In section 4, we prove the existence of self-similar profiles for different leading orders of $\rho(x,t)$ at the origin. In section 5, we analyze the far-field behavior of the self-similar profiles. In section 6, we present our numerical results.

2. Construction of the Near-field Solutions

In this section, we ignore the decay condition (1.8b), i.e. we use the local relation (1.8a) to replace the Biot-Savart law (1.6c) in the self-similar equations. We use a power series method to construct the self-similar profiles near $\xi = 0$, which we call the near-field solutions. Then we prove that the local solutions constructed in this way can be extended to whole $\mathbf{R}^+$.

We have the following Theorem

Theorem 2.1. *For fixed $c_l > 2$, there exist a family of non-trivial analytic solutions to the self-similar equations (1.6) (with (1.6c) replaced by (1.8a)) near $\xi = 0$, corresponding to different leading orders of $\rho(\xi)$ at $\xi = 0$, s, which is defined in (1.9).*

Proof. Assume

$$\rho(\xi) = \sum_{k=1}^{\infty} \rho_k \xi^k, \quad U(\xi) = \sum_{k=1}^{\infty} U_k \xi^k, \quad W(\xi) = \sum_{k=1}^{\infty} W_k \xi^k. \tag{2.1a}$$

Based on the local relation in the Biot-Savart law (1.8a), we have

$$W_k = k U_{k+1}. \tag{2.1b}$$

Plugging (2.1) into (1.6) and matching the k-th ($k \geq 1$) order term ξ^k, we get

$$(2 - c_l)\rho_k + k c_l \rho_k + \sum_{m=1}^{k-1} (k - m + 1)\rho_{k-m+1} U_m = 0, \tag{2.2a}$$

$$(k-1)U_k + c_l (k-1)^2 U_k + \sum_{m=1}^{k-1} U_m (k-m)^2 U_{k-m+1} - k\rho_k = 0, \tag{2.2b}$$

If initially the leading order of $\rho(x,0)$ at $x = 0$ is s, which is greater than 2 (1.2d), then according to (1.2b), s will remain as the leading order of $\rho(x,t)$ as long as the velocity field remains smooth. And as we discussed in Section 1, $\rho_x^{(s)}(x,t)$ should be positive near $x = 0$ to produce finite-time singularity. So in the corresponding self-similar profile (2.1a), there is

$$\rho_i = 0 \text{ for } i < s, \quad \rho_s > 0, \quad s \geq 2. \tag{2.3}$$

To make (2.2a) hold for $1 \leq k \leq s$, we require

$$(2 - c_l + s c_l + s U_1)\rho_s = 0. \tag{2.4}$$

Since $\rho_s \neq 0$, we require

$$U_1 = \frac{(1-s)c_l - 2}{s}. \tag{2.5}$$

To make (2.2b) hold for $1 \leq k < s$, we require

$$[(k-1) + c_l(k-1)^2 + U_1(k-1)^2]U_k = 0. \tag{2.6}$$

Since $c_l > 2$, and $[(k-1) + c_l(k-1)^2 + U_1(k-1)^2] > 0$, we require

$$U_k = 0, \quad 1 < k < s. \tag{2.7}$$

And to make (2.2b) hold for $k = s$, we require

$$U_s = \frac{s^2\rho_s}{sc_l - c_l - s + 2} > 0. \tag{2.8}$$

For $k > s$, to make (2.2) hold, the coefficients ρ_k and U_k should satisfy

$$\rho_k = \frac{-\sum_{m=s}^{k-1} U_m(k-m+1)\rho_{k-m+1}}{(k/s-1)(c_l-2)}, \tag{2.9a}$$

$$U_k = \frac{k\rho_k - \sum_{m=s}^{k-1} U_m(k-m)^2 U_{k-m+1}}{(k-1) + (c_l/s - 2/s)(k-1)^2}, \tag{2.9b}$$

which means the power series (2.1) can be determined inductively.

To complete the proof, we still need to verify that the constructed power series (2.1) converge for ξ small enough. We choose u^0, ρ^0 and r such that the following condition holds

$$|U_s| \leq \frac{1}{s^2}u^0 r^s, \quad |\rho_s| \leq \frac{1}{s}\rho^0 r^s, \quad \frac{(s+1)u^0 r}{c_l/s - 2/s} \leq 1, \quad \frac{9}{4}\frac{\rho^0/u^0 + u^0 r}{c_l/s - 2/s} < 1. \tag{2.10}$$

We can achieve this by choosing $u_0 r$ and ρ_0/u_0 small enough to make the last two hold, and then choosing r large enough to make the first two hold. For example, let

$$A = \min\{\frac{c_l - 2}{s(s+1)}, \frac{2(c_l-2)}{9s}\}, \ B = \frac{2(c_l-2)}{9s}, \ C = \max\{\frac{s\rho_s}{AB}, \frac{s^4\rho_s}{A(sc_l - c_l - s + 2)}\}. \tag{2.11}$$

Then the choice of

$$u_0 = \frac{A}{C^{1/(s-1)}}, \quad \rho_0 = u_0 B, \quad r = C^{1/(s-1)} \tag{2.12}$$

would satisfy (2.10). And we will use induction to prove that for all $k \geq s$,

$$|U_k| \leq \frac{1}{k^2}u^0 r^k, |\rho_k| \leq \frac{1}{k}\rho^0 r^k. \tag{2.13}$$

For $k = s$, (2.13) holds by (2.10). Assume now for $s \leq k < n$, (2.13) holds. Then for $k = n \geq s+1$, based on (2.9a) we have

$$|\rho_n| \leq \frac{\sum_{m=s}^{n-1} |U_m||(n-m+1)||\rho_{n-m+1}|}{(n-s)(c_l/s - 2/s)}. \tag{2.14}$$

Using the induction assumption and the fact that $\sum_{m=2}^{\infty} \frac{1}{m^2} \leq 1$, we have

$$|\rho_n| \leq \frac{\rho^0 u^0 r^{n+1}}{(n-s)(c_l/s - 2/s)} \leq \frac{\rho^0 r^n}{n} \times \frac{(s+1)u^0 r}{c_l/s - 2/s} \leq \frac{\rho^0 r^n}{n}, \tag{2.15}$$

where we have used the fact $n \geq s+1$ in the second inequality and (2.10) in the third inequality. Thus (2.13) holds for ρ_n. Based on (2.9b), we have

$$|U_n| \leq \frac{|n\rho_n| + \sum_{m=s}^{n-1} |U_m(n-m)^2||U_{n-m+1}|}{(c_l/s - 2/s)(n-1)^2} \tag{2.16}$$

Using the induction assumption and the fact that $\sum_{m=2}^{\infty} \frac{1}{m^2} \leq 1$, we get

$$|U_n| \leq \frac{\rho^0 r^n + (u^0)^2 r^{n+1}}{(c_l/s - 2/s)(n-1)^2} \leq \frac{u_0 r^n}{n^2} \times \frac{\rho_0/u_0 + u_0 r}{c_l/s - 2/s} \times \frac{n^2}{(n-1)^2} \leq \frac{u_0 r^n}{n^2}, \tag{2.17}$$

where we have used (2.10) and the fact that $n \geq 3$, $n^2/(n-1)^2 \leq 9/4$ in the last inequality.

So we just proved (2.13) by induction, which implies the power series (2.1) converge in some short interval $[0, 1/r)$. This completes the proof of Theorem 2.1. □

Remark 2.1. *We require $c_l > 2$ in Theorem 2.1. If $c_l = 2$, there exist only trivial solutions to (1.6). If $c_l < 2$, then $c_\rho < 0$ according to (1.5), which means $\rho(x,t)$ blows up in finite time according to (1.4). This is impossible since $\rho(x,t)$ is transported by the fluid.*

Remark 2.2. *For fixed c_l, we have one degree of freedom $\rho_s > 0$ in constructing the near-field solutions (2.1), which can be easily verified to play the role of a scaling parameter (1.7). We will simply choose $\rho_s = 1$ in our argument for the rest part of this paper.*

The power series (2.1) we construct only converge in a short interval near $\xi = 0$. However, these local self-similar profiles can be extended to $+\infty$.

Theorem 2.2. *For $c_l > 2$, the analytic solutions (2.1) we construct can be extended to the whole $\mathbf{R}^+$, resulting in solutions to the self-similar equations (1.6) with (1.6c) replaced by (1.8a). Moreover, we have for $\xi > 0$,*

$$W(\xi) > 0, \quad \rho(\xi) > 0. \tag{2.18}$$

Proof. Since $c_l + U_1 = (c_l - 2)/s > 0$, $\rho_s > 0$, $W_s = (s-1)U_s > 0$, based on the leading orders of the power series (2.1), we can choose $\epsilon < \frac{1}{r}$ small enough such that

$$c_l\epsilon + U(\epsilon) > 0, \quad W(\epsilon) > 0, \quad \rho(\epsilon) > 0. \tag{2.19}$$

Then we consider extending the self-similar profiles from $\xi = \epsilon$ to $+\infty$ by solving an ODE system with initial conditions given by the power series (2.1). Let $\tilde{U}(\xi) = c_l\xi + U(\xi)$, then according to (1.6), $\tilde{U}(\xi)$, $\rho(\xi)$ and $U(\xi)$ satisfy the following ODE

$$\rho'(\xi) = \frac{(c_l - 2)\rho(\xi)}{\tilde{U}(\xi)}, \tag{2.20a}$$

$$W'(\xi) = \frac{(c_l - 2)\rho(\xi)}{\tilde{U}(\xi)^2} - \frac{W(\xi)}{\tilde{U}(\xi)}, \tag{2.20b}$$

$$(\frac{\tilde{U}(\xi)}{\xi})' = \frac{W(\xi)}{\xi}. \tag{2.20c}$$

The right hand side of (2.20) is locally Lipschitz continuous for $\tilde{U}(\xi) \neq 0$, $\xi \neq 0$, so we can solve the ODE system from ϵ and get its solution on interval $[\epsilon, T)$. We first prove that $W(\xi)$ is positive on $[\epsilon, T)$. Otherwise denote $\xi = t$ as the first time $W(\xi)$ reaches 0, i.e.

$$t = \inf\{s \in [\epsilon, T) : W(s) \leq 0\}. \tag{2.21}$$

Then we have $W(\xi)$ is positive on $[\epsilon, t)$, and

$$W'(t) \leq 0. \tag{2.22}$$

Based on (2.20c), $\frac{\tilde{U}(\xi)}{\xi}$ is increasing on $[\epsilon, t)$, thus $\tilde{U}(\xi) > \tilde{U}(\epsilon) > 0$ for $\xi \in [\epsilon, t]$. Then based on (2.20a), $\rho(\xi)$ is increasing on $[\epsilon, t]$, and $\rho(t) > 0$. Evaluating (2.20b) at $\xi = t$, we get

$$W'(t) = \frac{(c_l - 2)\rho(t)}{\tilde{U}(t)^2} > 0, \tag{2.23}$$

which contradicts with (2.22). So $W(\xi) > 0$ and consequently $\rho(\xi) > 0$ for $\xi \in [\epsilon, T)$.

Using the fact that $W(\xi) > 0$ in (2.20c), we have for $\xi > \epsilon$,

$$\tilde{U}(\xi) \geq C_0 \xi. \tag{2.24}$$

Using this lower bound in (2.20a), we get

$$\rho'(\xi) \leq \frac{C_1 \rho(\xi)}{\xi}. \tag{2.25}$$

This implies that for $\xi > \epsilon$

$$\rho(\xi) \leq C_2 \xi^{C_1}. \tag{2.26}$$

Using (2.26), (2.24) and the fact that $W(\xi)$ is positive in (2.20b), we have

$$W'(\xi) \leq C_3 \xi^{C_1 - 2}. \tag{2.27}$$

Thus for $\xi > \epsilon$,

$$W(\xi) \leq C_4 \xi^{C_1}. \tag{2.28}$$

Finally using (2.28) in (2.20c), we get for $\xi > \epsilon$,

$$U(\xi) \leq C_5 \xi^{C_1 + 2}. \tag{2.29}$$

The C_0, C_1,... C_5 in the above estimates are positive constants. These *a priori* estimates (2.24), (2.29), (2.26) and (2.28) together imply that we can get solutions to (2.20) on $[\epsilon, +\infty)$, i.e. the local self-similar profile constructed using power series can be extended to $+\infty$. □

3. Determination of the Scaling Exponents

In our construction of self-similar profiles in the previous section, we did not consider the decay condition (1.8b). In this section, we prove that the decay condition determines the scaling exponent c_l, i.e. only for certain c_l does the decay condition hold.

Recall that for a fixed leading order of $\rho(\xi)$, the self-similar profiles $U(\xi)$, $\rho(\xi)$ and $W(\xi)$ depend on the scaling exponent c_l only. So we can define a function $G(c_l)$ as

$$G(c_l) = \lim_{\xi \to +\infty} \frac{U(\xi)}{\xi}. \tag{3.1}$$

We will prove that $G(c_l) < +\infty$ and it is a continuous function of c_l. Then the existence of c_l to satisfy the decay condition (1.8b) will follow from the Intermediate Value Theorem if we can show that there exist c_l^l and c_l^r such that

$$G(c_l^l) < 0, \quad G(c_l^r) > 0. \tag{3.2}$$

Theorem 3.1. *For a fixed leading order of $\rho(\xi)$, s, and a scaling exponent $c_l > 2$, construct the power series (2.1) with $\rho_s = 1$ and extend the profiles to $\mathbf{R}^+$. Then the limit*

$$G(c_l) = \lim_{\xi \to \infty} \frac{U(\xi)}{\xi} < +\infty, \tag{3.3}$$

and $G(c_l)$ is a continuous function of c_l.

We first make the following change of variables,

$$\eta = \xi^{1/c_l}, \quad \hat{W}(\eta) = W(\xi), \quad \hat{U}(\eta) = U(\xi)\xi^{-1}, \quad \hat{\rho}(\eta) = \rho(\xi)\xi^{-1+2/c_l}. \tag{3.4}$$

Then we have

$$G(c_l) = \lim_{\eta \to +\infty} \hat{U}(\eta), \tag{3.5}$$

and the ODE system satisfied by $\hat{U}(\eta), \hat{\rho}(\eta), \hat{W}(\eta)$ is

$$\hat{\rho}'(\eta) = \frac{(2/c_l - 1)\hat{\rho}(\eta)\hat{U}(\eta)}{\eta + 1/c_l \hat{U}(\eta)\eta}, \tag{3.6a}$$

$$\hat{W}'(\eta) = \frac{-\hat{W}(\eta)}{\eta + 1/c_l \hat{U}(\eta)\eta} + \frac{(1 - 2/c_l)\hat{\rho}(\eta)}{(1 + 1/c_l \hat{U}(\eta))^2 \eta^3}, \tag{3.6b}$$

$$\hat{U}'(\eta) = \frac{c_l \hat{W}(\eta)}{\eta}. \tag{3.6c}$$

According to (2.5), (2.18) and the fact that $\hat{U}(\eta)$ is monotone increasing, we have

$$\hat{U}(\eta) > \hat{U}(0) = \frac{(1-s)c_l - 2}{s}, \quad \hat{W}(\eta) > 0, \quad \hat{\rho}(\eta) > 0, \quad \text{for} \quad \eta > 0. \tag{3.7}$$

Before proving Theorem 3.1, we will first prove the following two Lemmas.

Lemma 3.1. *For all $c_l > 2$, $G(c_l) > -2$.*

Proof. Assume that for some $c_l > 2$, $G(c_l) \leq -2$. Then according to (3.7) and the fact that $\hat{U}(\eta)$ is increasing, we have for all $\eta > 0$,

$$\frac{(1-s)c_l - 2}{s} < \hat{U}(\eta) < -2. \tag{3.8}$$

Then we get

$$\frac{(2/c_l - 1)\hat{U}(\eta)}{1 + 1/c_l \hat{U}(\eta)} \geq 2. \tag{3.9}$$

It follows from (3.6a) that

$$\hat{\rho}'(\eta) \geq 2\frac{\hat{\rho}(\eta)}{\eta}. \tag{3.10}$$

By direct integration and (3.7), we have for η large enough,

$$\hat{\rho}(\eta) \geq C_1 \eta^2. \tag{3.11}$$

Using this estimate in (3.6b), we get

$$\hat{W}'(\eta) \geq -\frac{C_2 \hat{W}(\eta)}{\eta} + \frac{C_3}{\eta}. \tag{3.12}$$

This implies

$$\left(\eta^{C_2}\hat{W}(\eta)\right)' \geq C_3\eta^{C_2-1}. \tag{3.13}$$

Then we have for η large enough,

$$\eta^{C_2}\hat{W}(\eta) \geq \frac{C_3}{C_2}\eta^{C_2} - C_4. \tag{3.14}$$

Using this lower bound in (3.6c), we will get

$$\hat{U}'(\eta) \geq \frac{C_5}{\eta} - \frac{C_6}{\eta^{C_2+2}}. \tag{3.15}$$

The constants C in the above estimates are positive and independent of η. The inequality (3.15) implies that $\hat{U}(\eta) \to +\infty$ as $\eta \to +\infty$, which contradicts with $G(c_l) \leq -2$. This completes the proof of Lemma 3.1. □

We add a subscript c_l to indicate the dependence of the profiles on c_l for the rest part of this section:

$$\hat{U}_{c_l}(\eta) = \hat{U}(\eta),\ \hat{W}_{c_l}(\eta) = \hat{W}(\eta),\ \hat{W}_{c_l}(\eta) = \hat{W}(\eta). \tag{3.16}$$

Lemma 3.2. *For fixed $\eta > 0$, $\hat{U}_{c_l}(\eta)$, $\hat{W}_{c_l}(\eta)$ and $\hat{\rho}_{c_l}(\eta)$ are continuous functions of c_l.*

Proof. We only need to prove that for fixed $c_l^0 > 2$, $\hat{U}_{c_l}(\eta)$, $\hat{\rho}_{c_l}(\eta)$ and $\hat{W}_{c_l}(\eta)$ as functions of c_l are continuous at $c_l = c_l^0$. In our construction of the power series using (2.9), we can easily see that the coefficients U_k and ρ_k depend continuously on c_l. And based on the condition (2.10), there exist uniform upper bounds of these coefficients

$$|U_k| \leq \frac{u^0 r^k}{k^2}, \quad |\rho_k| \leq \frac{\rho^0 r^k}{k}, \tag{3.17}$$

for c_l in a neighbourhood of c_l^0. This means there exists a fixed ϵ small enough, such that $\hat{W}_{c_l}(\epsilon)$, $\hat{\rho}_{c_l}(\epsilon)$ and $\hat{U}_{c_l}(\epsilon)$ are continuous at c_l^0. Then we use the continuous dependence of ODE solutions on initial conditions and parameter to complete the proof of this Lemma. □

Now we begin to prove Theorem 3.1. We use an iterative method which enables to get shaper estimates of the profiles after each iteration. We finally attain that $\hat{U}_{c_l}(\eta)$ converges uniformly to $G(c_l)$, with which we can complete the proof of this Theorem.

Proof. Consider $c_l^0 > 2$, we will prove that $G(c_l^0) < +\infty$, and $G(c_l)$ is continuous at $c_l = c_l^0$.

According to Lemma 3.1 and Lemma 3.2, there exists η_0 large enough and a neighborhood of c_l^0, $I_0 = (c_1, c_2)$ with $c_1 > 2, c_2 < +\infty$ such that for $c_l \in I_0$ and $\eta > \eta_0$,

$$\hat{U}_{c_l}(\eta) > \hat{U}_{c_l}(\eta_0) > -2 + \epsilon_1. \tag{3.18}$$

Then for $c_l \in I_0$ and $\eta > \eta_0$, there exist $\epsilon_2 > 0$, such that

$$\frac{(2/c_l - 1)\hat{U}_{c_l}(\eta)}{1 + 1/c_l\hat{U}_{c_l}(\eta)} < 2 - \epsilon_2. \tag{3.19}$$

Using this in (3.6a), we have for $c_l \in I_0$ and $\eta > \eta_0$,

$$\hat{\rho}'_{c_l}(\eta) \leq \frac{(2-\epsilon_2)\hat{\rho}_{c_l}(\eta)}{\eta}. \tag{3.20}$$

Using direct integration and Lemma 3.2, we have for $c_l \in I_0$, $\eta > \eta_0$,

$$\hat{\rho}_{c_l}(\eta) \leq C_1\eta^{2-\epsilon_2}. \tag{3.21}$$

Using this upper bound of $\hat{\rho}(\eta)$ in (3.6b), we have for $c_l \in I_0$, $\eta > \eta_0$,

$$\hat{W}'_{c_l}(\eta) \leq \left(\frac{-1}{1 + 1/c_l \hat{U}_{c_l}(\eta)} \right) \frac{\hat{W}_{c_l}(\eta)}{\eta} + C_3 \eta^{-1-\epsilon_2}. \tag{3.22}$$

The first term in (3.22) is negative according to (3.7) and the second term is integrable for $\eta > \eta_0$. Then using Lemma 3.2, we have for $c_l \in I_0$, $\eta > \eta_0$,

$$\hat{W}_{c_l}(\eta) < C_4 \tag{3.23}$$

Putting this upper bound in (3.6c) and using Lemma 3.2, we get for $c_l \in I_0$, $\eta > \eta_0$,

$$\hat{U}_{c_l}(\eta) < C_5 \ln \eta. \tag{3.24}$$

Putting this upper bound of $\hat{U}(\eta)$ back in (3.6b), we have for $c_l \in I_0$, $\eta > \eta_0$

$$\hat{W}'_{c_l}(\eta) < -\frac{C_6 \hat{W}_{c_l}(\eta)}{\eta \ln \eta} + C_3 \eta^{-1-\epsilon_2}, \tag{3.25}$$

which by direct integration gives that for $c_l \in I_0$, $\eta > \eta_0$,

$$\hat{W}_{c_l}(\eta) \exp\Big(\int_{\eta_0}^{\eta} \frac{C_6}{\zeta \ln \zeta} \mathrm{d}\zeta \Big) < C_7. \tag{3.26}$$

Thus we have for $c_l \in I_0$ and $\eta > \eta_0$,

$$\hat{W}_{c_l}(\eta) < C_8 / \ln \eta. \tag{3.27}$$

Using this sharper upper bound of $W(\eta)$ in (3.6c), we get for $c_l \in I_0$, $\eta > \eta_0$,

$$\hat{U}_{c_l}(\eta) < C_9 \ln \ln \eta. \tag{3.28}$$

Again putting this sharper upper bound in (3.6b), we have for $c_l \in I_0$, $\eta > \eta_0$,

$$\hat{W}'_{c_l}(\eta) < -\frac{C_{10} \hat{W}_{c_l}(\eta)}{\eta \ln \eta} + C_3 \eta^{-1-\epsilon_2}, \tag{3.29}$$

By direct integration, we get

$$\hat{W}_{c_l}(\eta) \exp\Big(\int_{\eta_0}^{\eta} \frac{C_{11}}{\zeta \ln \ln \zeta} \mathrm{d}\zeta \Big) < C_{12}. \tag{3.30}$$

Since $\int_{\eta_0}^{\eta} \frac{C_{11}}{\zeta \ln \ln \zeta} \mathrm{d}\zeta > C_{13} (\ln \eta)^{\alpha}$ for some $\alpha \in (0,1)$, we have for $c_l \in I_0$, $\eta > \eta_0$,

$$\hat{W}_{c_l}(\eta_1) < C_{14} \exp\big(- C_{13} (\ln \eta)^{\alpha} \big). \tag{3.31}$$

Note that $C_1, C_2, \ldots C_{14}$ in the above estimates are all positive constants in dependent of η. Using the upper bound of $\hat{W}_{c_l}(\eta)$ (3.31) in (3.6c) we conclude that $\hat{U}_{c_l}(\eta)$ converges uniformly as $\eta \to +\infty$ for $c_l \in I_0$ and complete the proof of this Theorem. □

To complete the proof of our main result Theorem 1.1, we still need to verify condition (3.2) for different s. And we leave this part to section 4.

4. Existence of Self-Similar Profiles

In this section, we verify that condition (3.2) holds for several $s \geq 2$, i.e., there exist c_l^l and $c_l^r > 2$, such that $G(c_l^l) < 0,\ G(c_l^r) > 0$, with which we can complete the proof of Theorem 1.1. We will use the following Lemma, which allows us to prove (3.2) using only estimates of the profiles at some fixed η_0.

Lemma 4.1. *Consider solving equations (3.6) with initial conditions given by power series (2.1). For some $\eta_0 > 0$, let $u_0 = \hat{U}(\eta_0)$, $\rho_0 = \hat{\rho}(\eta_0)$, $w_0 = \hat{W}(\eta_0)$.*
If

$$u_0 > 0, \tag{4.1a}$$

then we have

$$G(c_l) > 0. \tag{4.1b}$$

If

$$u_0 > -2, \quad u_0 + c_l w_0 + \frac{(c_l - 2)\rho_0}{(u_0 + 2)(1 + u_0/c_l)} < 0, \tag{4.1c}$$

Then

$$G(c_l) < 0. \tag{4.1d}$$

Proof. Since $G(c_l) = \lim_{\eta \to +\infty} \hat{U}(\eta)$, and $\hat{U}(\eta)$ is increasing according to (3.6c) and (2.18), so if $u_0 > 0$, then $G(c_l) > u_0 > 0$, and we finish the first part of the Lemma (4.1b).

We prove the second part by contradiction. If $G(c_l) \geq 0$, there exists $\eta_1 \in (\eta_0, +\infty]$ such that $\hat{U}(\eta_1) = 0$. Then for $\eta \in (\eta_0, \eta_1)$, $\hat{U}(\eta) > u_0$, and according to (3.6a) we have,

$$\hat{\rho}'(\eta) \leq \frac{(2/c_l - 1)u_0}{1 + u_0/c_l} \frac{\hat{\rho}(\eta)}{\eta}. \tag{4.2a}$$

By direct integration, we get for $\eta \in (\eta_0, \eta_1)$,

$$\hat{\rho}(\eta) \leq \rho^0 \eta_0^{\frac{(1-2/c_l)u_0}{1+u_0/c_l}} \eta^{\frac{(2/c_l-1)u_0}{1+u_0/c_l}}. \tag{4.2b}$$

Using this upper bound of $\hat{\rho}$ and the fact that $\hat{U}(\eta) < 0$ for $\eta \in (\eta_0, \eta_1)$ in (3.6b), we get

$$(\hat{W}(\eta)\eta)' \leq \frac{1 - 2/c_l}{(1 + u_0/c_l)^2} \rho_0 \eta_0^{\frac{(1-2/c_l)u_0}{1+u_0/c_l}} \eta^{\frac{-u_0-2}{1+u_0/c_l}}. \tag{4.3a}$$

Since $u_0 > -2$, integrating (4.3a) from η_0 to η, we have for $\eta \in (\eta_0, \eta_1)$

$$\hat{W}(\eta)\eta \leq w_0\eta_0 + \frac{2/c_l - 1}{(1 + u_0/c_l)(u_0/c_l - u_0 - 1)} \rho_0 (\eta_0^{-1} - \eta_0^{\frac{(1-2/c_l)u_0}{1+u_0/c_l}} \eta^{\frac{-u_0-1+u_0/c_l}{1+u_0/c_l}}). \tag{4.3b}$$

Putting this upper bound of $\hat{W}(\eta)$ in (3.6c) and integrating it from η_0 to η_1, we get

$$0 - u_0 = \hat{U}(\eta_1) - \hat{U}(\eta_0) \leq c_l w_0 + \frac{(c_l - 2)\rho_0}{(u_0 + 2)(1 + u_0/c_l)}, \tag{4.4}$$

which contradicts (4.1c), and we complete the proof of this Lemma. □

We will use numerical computation and rigorous error estimation to verify condition (4.1a) or (4.1c). We first numerically construct the power series (2.1) and then extend the local self-similar profiles to some η_0 by numerically solving an ODE system.

Note that in equations (3.6), there are $1/\eta^3$ terms in the right hand side, which can be very large for small η. This will make the numerical solutions sensitive to roundoff error. So instead of solving (3.6) directly, we make the following change of variables,

$$\tilde{\rho}(\eta) = \hat{\rho}(\eta)\eta^{-5}, \quad \tilde{W}(\eta) = \hat{W}(\eta)\eta^{-1}, \quad \tilde{U}(\eta) = \hat{U}(\eta), \tag{4.5}$$

and the equations satisfied by this new set of unknowns are given by

$$\tilde{\rho}'(\eta) = \frac{(-3-c_l)\tilde{\rho}(\eta)\tilde{U}(\eta) - 5c_l\tilde{\rho}(\eta)}{c_l\eta + \tilde{U}(\eta)\eta}, \tag{4.6a}$$

$$\tilde{W}'(\eta) = \frac{-2c_l\tilde{W}(\eta) - \tilde{U}(\eta)\tilde{W}(\eta)}{c_l\eta + \tilde{U}(\eta)\eta} + \frac{c_l(c_l-2)\tilde{\rho}(\eta)\eta}{(c_l + \tilde{U}(\eta))^2}, \tag{4.6b}$$

$$\tilde{U}'(\eta) = c_l\tilde{W}(\eta). \tag{4.6c}$$

After this change of variables, there are only $1/\eta$ terms for this new system of ODEs.

We demonstrate how to rigorously bound the numerical error of the self-similar profiles at η_0 through the case $s = 2$, but the same procedure can be applied to other s to prove the existence of self-similar profiles. For the case $s = 2$, we choose $c_l^l = 3$ and $c_l^r = 8$ in (3.2).

4.1. **The case $s = 2$, $c_l = 3$.** We need to go though the following several steps.

Step 1 We need to bound the truncation error of the power series (2.1). To numerically compute the power series (2.1), we first truncate the power series to certain terms, and the truncation error can be bounded using (2.13). For the case $s = 2$, $c_l = 3$, it can be easily verified that the following choice of ρ^0, u^0 and r makes (2.10) hold:

$$u^0 = \frac{1}{9\times 162}, \quad \rho^0 = \frac{1}{9\times 9\times 162}, \quad r = 162. \tag{4.7}$$

Based on (4.5) and (2.1), at $\xi = 10^{-3}$, corresponding to $\eta_s = 10^{-1}$, we have

$$\tilde{U}(\eta_s) = \sum_{k=1}^{\infty} U_k\eta^{3k-3}, \quad \tilde{\rho}(\eta_s) = \sum_{k=2}^{\infty}\rho_k\eta^{3k-6}, \quad \tilde{W}(\eta_s) = \sum_{k=1}^{\infty} W_k\eta^{3k-1}. \tag{4.8}$$

Using estimate (2.13), if we truncate the series (4.8) at $k = 20$, the truncation error for all the three series can be bounded by 10^{-15}. We will numerically compute

$$\tilde{U}(\eta_s) \approx \sum_{k=1}^{20} U_k\eta^{3k-3}, \quad \tilde{\rho}(\eta_s) \approx \sum_{k=2}^{20}\rho_k\eta^{3k-6}, \quad \tilde{W}(\eta_s) \approx \sum_{k=1}^{20} W_k\eta^{3k-1}. \tag{4.9}$$

and use them as initial conditions to solve (4.6).

Step 2 We need to bound the roundoff error in computing the truncated power series (4.9). Denote fl as the floating point operation and assume a and b are two floating point numbers, which can be stored exactly on computer. Then by the IEEE standard rounding off rules [12], we have if $fl(a \odot b) \neq 0$,

$$\mathrm{fl}(a \odot b) = (a \odot b)(1+\delta), \quad |\delta| \leq \epsilon, \tag{4.10}$$

where $\odot$ can be $+$, $-$, $\times$ and $\div$, and ϵ is the machine precision. When using double precision floating point operation on matlab, there is

$$\epsilon < 3\times 10^{-15}. \tag{4.11}$$

The following two Lemmas will be intensively used to control the roundoff error.

Lemma 4.2. *Assuming a and b are two floating point numbers stored in the computer, then we have the following upper and lower bounds,*
if $\mathrm{fl}(a \odot b) > 0$,

$$a \odot b \le \mathrm{fl}\Big(\mathrm{fl}(a \odot b) \times \mathrm{fl}\big(1 + \mathrm{fl}(4\epsilon)\big)\Big), \quad a \odot b \ge \mathrm{fl}\Big(\mathrm{fl}(a \odot b) \times \mathrm{fl}\big(1 - \mathrm{fl}(4\epsilon)\big)\Big), \tag{4.12a}$$

if $\mathrm{fl}(a \odot b) < 0$,

$$a \odot b \le \mathrm{fl}\Big(\mathrm{fl}(a \odot b) \times \mathrm{fl}\big(1 - \mathrm{fl}(4\epsilon)\big)\Big), \quad a \odot b \ge \mathrm{fl}\Big(\mathrm{fl}(a \odot b) \times \mathrm{fl}\big(1 + \mathrm{fl}(4\epsilon)\big)\Big). \tag{4.12b}$$

The RHS of the inequaltities (4.12) only involve floating point operation, which implies that even though we cannot get the exact answer because of the roundoff error, we can get rigorous lower and upper bounds of the answer using only floating point operation. The basic idea in the above lower and upper bounds is compensating the roundoff error by multiplying $(1 \pm n\epsilon)$. Since ϵ is very small, these lower and upper bounds are actually very tight. We only prove the upper bound in (4.12a) for the case $\odot$ is '+'. Others are similar.

Proof. According to the rounding rule (4.10),

$$\mathrm{fl}\Big(\mathrm{fl}(a+b) \times \mathrm{fl}\big(1 + \mathrm{fl}(4\epsilon)\big)\Big) = \mathrm{fl}\Big((a+b)(1+\delta_1) \times \mathrm{fl}\big(1 + 4\epsilon(1+\delta_2)\big)\Big) \tag{4.13}$$

$$= \mathrm{fl}\Big((a+b)(1+\delta_1) \times (1+\delta_3)\big(1 + 4\epsilon(1+\delta_2)\big)\Big) \tag{4.14}$$

$$= (a+b)(1+\delta_1)(1+\delta_3)(1+\delta_4)(1+4\epsilon+4\epsilon\delta_2) \tag{4.15}$$

$$\ge (a+b). \tag{4.16}$$

In the last inequality we have used $|\delta_1|$, $|\delta_2|$, $|\delta_3|$, $|\delta_4| \le \epsilon$. □

Lemma 4.3. *Assuming we have lower and upper bounds of a and b,*

$$a^{\max}, \quad a^{\min}, \quad b^{\max}, \quad b^{\min}. \tag{4.17}$$

Let

$$V = \{a^{\max} \odot b^{\max}, a^{\max} \odot b^{\min}, a^{\min} \odot b^{\max}, a^{\min} \odot b^{\min}\}, \tag{4.18}$$

then

$$a \odot b \le \sup V, \quad a \odot b \ge \inf V, \tag{4.19}$$

where $\odot$ can be $+$, $-$, $\times$ and $\div$. When $\odot$ is $\div$, we require $0 \notin [b^{\min}, b^{\max}]$.

Lemma 4.3 is obvious, so we omit its proof here.

Remark 4.1. *Lemma 4.12 and Lemma 4.3 allow us to rigorously control the roundoff error introduced in our numerical computation: Assuming we have lower and upper bounds of a and b, which are floating point numbers stored exactly on computer. Then we can use Lemma 4.2 to get lower and upper bounds for each element of (4.18). Then putting these bounds together in (4.19) and using Lemma 4.3, we can get rigorous bounds of $a \odot b$. The numerical computations involved in this paper are all composed of these 4 basic arithmetic operations, so by using the two Lemmas in each single step of our computation, we can rigorously bound the roundoff error in our final results.*

When computing the truncated power series (4.9), we need to first compute the coefficients U_k and ρ_k based on (2.9). The relation (2.9), Lemma 4.3 and Lemma 4.2 together allow us to get lower and upper bounds of the coefficients U_k and ρ_k inductively: Assuming now we have got lower and upper bounds of U_m and ρ_m for $m < k$, which are all floating point

numbers, then based on (2.9a), and using Lemma 4.2 and Lemma 4.3 in each single step of the computation, we can get lower and upper bounds of ρ_k. Then we use the same technique in (2.9b) to get lower and upper bounds of U_k.

After getting the upper and lower bounds of ρ_k and U_k for all $k \leq 20$, we use Lemma 4.3 and Lemma 4.2 in computing (4.9), and get lower and upper bounds of the truncated power series. Based on our computation, the difference of the lower bounds and upper bounds are all less than 5×10^{-14}, which means if we use the upper bounds to approximate the real values of the truncated power series (4.9), the numerical errors are less than 5×10^{-14}. We denote the upper bounds of the truncated power series (4.9) as

$$\tilde{y}_0 = (\tilde{w}_0, \tilde{u}_0, \tilde{\rho}_0)^T. \tag{4.20}$$

Since the truncation error of the power series are less than 10^{-15}, we get a rigorous error bound of the self-similar profiles (4.20) at $\eta_s = 0.1$, which we denote by $E_0 = (E_0^w, E_0^u, E_0^\rho)^T$,

$$E_0 = (10^{-13}, 10^{-13}, 10^{-13})^T. \tag{4.21}$$

We will use (4.20) and (4.21) as initial conditions to numerically solve (4.6).

Step 3 We need to bound the numerical error introduced in numerically solving (4.6). We will use the forward Euler method with step size $h = 2.9 \times 10^{-6}$ to solve (4.6) from $\eta_s = 10^{-1}$ to $\eta_0 = 3$. We denote the node point and numerical solutions at the n-th step as

$$x_n = 0.1 + nh, \quad \tilde{y}_n = (\tilde{u}_n, \tilde{\rho}_n, \tilde{w}_n)^T, \quad n = 0, \ldots, 10^6, \tag{4.22}$$

and the exact solutions and error bounds at the n-th step as

$$y_n = (u_n, \rho_n, w_n)^T, \quad E_n = (E_n^w, E_n^u, E_n^\rho)^T, \quad n = 0, \ldots 10^6, \tag{4.23}$$

which means

$$|y_n - \tilde{y}_n| \leq E^n. \tag{4.24}$$

Based on the previous step, $\tilde{y}_0$ and E^0 given by (4.20) and (4.21). Our approach to bound the error introduced in numerically solving (4.6) is simultaneously tracking $\tilde{y}_n$ and E^n, i.e. in each step of the forward Euler method we update $\tilde{y}_n$ and E^n together,

$$(\tilde{y}_n, E^n) \to (\tilde{y}_{n+1}, E^{n+1}). \tag{4.25}$$

Denoting $f = (f_w, f_u, f_\rho)^T$ as the RHS of (4.6), the forward Euler method gives

$$\tilde{w}_{n+1} = \tilde{w}_n + f_w(\tilde{w}_n, \tilde{u}_n, \tilde{\rho}_n, x_n)h + e^w_{\text{roundoff}}, \tag{4.26a}$$

$$\tilde{u}_{n+1} = \tilde{u}_n + f_u(\tilde{w}_n, \tilde{u}_n, \tilde{\rho}_n)h + e^u_{\text{roundoff}}, \tag{4.26b}$$

$$\tilde{\rho}_{n+1} = \tilde{\rho}_n + f_\rho(\tilde{w}_n, \tilde{u}_n, \tilde{\rho}_n)h + e^\rho_{\text{roundoff}}. \tag{4.26c}$$

For the exact solutions at x_n and x_{n+1} which are y_n and y_{n+1}, we have

$$w_{n+1} = w_n + f_w(w_n, u_n, \rho_n, x_n)h + 1/2\tilde{W}''(w^1, u^1, \rho^1, x^1)h^2, \tag{4.27a}$$

$$u_{n+1} = u_n + f_u(w_n, u_n, \rho_n, x_n)h + 1/2\tilde{U}''(w^2, u^2, \rho^2, x^2)h^2, \tag{4.27b}$$

$$\rho_{n+1} = \rho_n + f_\rho(w_n, u_n, \rho_n, x_n)h + 1/2\tilde{\rho}''(w^3, u^3, \rho^3, x^2)h^2, \tag{4.27c}$$

where $x^i \in (x_n, x_{n+1})$, $w^i = \tilde{W}(x^i)$, $\rho^i = \tilde{\rho}(x^i)$, $u^i = \tilde{U}(x^i)$, $i = 1, 2, 3$.

Deducting (4.26a) from (4.27), we get

$$y_{n+1} - \tilde{y}_{n+1} = (I + Ah)(y_n - \tilde{y}_n) + \frac{1}{2}y''(w^i, u^i, \rho^i, x^i)h^2 - e_{\text{roundoff}}. \tag{4.28}$$

where A is the gradient of the RHS f with respect to (w, u, ρ),

$$A = \nabla f(x_n, w^4, u^4, \rho^4) \tag{4.29}$$

$$= \begin{pmatrix} \frac{-2c_l-u^4}{c_l x^n+u^4 x_n} & \frac{c_l^2(w^4-2x_n^2\rho^4)+4c_l\rho^4x_n^2+c_l u^4 w^4}{(u^4+c_l)^3 x_n} & \frac{c_l(c_l-2)x_n}{(c_l+u^4)^2} \\ c_l & 0 & 0 \\ 0 & -\frac{c_l(c_l-2)\rho^4}{(c_l+u^4)^2\eta} & -\frac{c_l(u^4+5)+3u^4}{(c_l+u^4)x^n} \end{pmatrix} \tag{4.30}$$

with $y^4 = (w^4, u^4, \rho^4)$ lies within the numerical solution $\tilde{y}_n$ and real solution y_n.

So we get a rigorous error bound at the $n+1$-st step,

$$|y_{n+1} - \tilde{y}_{n+1}| \le |I + Ah| E_n + \frac{h^2}{2}|y''(w^i, u^i, \rho^i, x^i)| + |e_{\text{roundoff}}| \tag{4.31}$$

$$= I_1 + I_2 + I_3, \tag{4.32}$$

where $I_1 = |I+Ah|E_n$ is the propagation of error from the previous step, $I_2 = h^2/2|y''(y^i, x^i)|$ is the local truncation error, and I_3 is the roundoff error in computing $\tilde{y}_{n+1}$ in (4.26a).

Step 4 We first consider the first part I_1. We can get lower and upper bounds of y^4 using $|y^4 - \tilde{y}_n| \le E_n$, Lemma 4.3 and Lemma 4.2. Since A is explicitly given by (4.29), we can get lower and upper bounds for each entry of $I + Ah$ using Lemma 4.3 and Lemma 4.2. The strategy is the same as *Step 2* and we omit the details here. Taking absolute value for these lower and upper bounds, we get upper bounds for $|I + Ah|$. Then we use Lemma 4.3 and Lemma 4.2 in computing $|I + Ah|E_n$ and finally get rigorous upper bound of I_1.

Step 5 Then we consider the second part I_2. To bound the local truncation error I_2, we need to bound the second order derivatives of the solutions on the interval $[x_n, x_{n+1}]$. For $c_l = 3$ we have

$$\tilde{\rho}''(\eta) = \frac{3\tilde{\rho}(90 + 71\tilde{U} + 14\tilde{U}^2 - 3\eta\tilde{W})}{\eta^2(3+\tilde{U})^2}, \tag{4.33a}$$

$$\tilde{W}''(\eta) = \frac{-18\eta^2\tilde{\rho}(\eta)(3+\tilde{U}+\eta\tilde{W}) + (3+\tilde{U})\tilde{W}(54+21\tilde{U}+2\tilde{U}^2+9\eta\tilde{W})}{\eta^2(3+\tilde{U})^3}, \tag{4.33b}$$

$$\tilde{U}''(\eta) = \frac{9\eta^2\tilde{\rho} - 3(18+9\tilde{U}+\tilde{U}^2)W}{\eta(3+\tilde{U})^2}. \tag{4.33c}$$

We need the following *a priori* estimates to bound (4.33).

Lemma 4.4. *Consider the ODE system (4.6) with initial conditions given by power series (2.1), assume at η_0, the solutions are $\tilde{U}(\eta_0)$, $\tilde{W}(\eta_0)$, $\tilde{\rho}(\eta_0)$, then for $\eta \in [\eta_0, \eta_0 + h]$, we have the following* a priori *estimates*

$$\tilde{\rho}(\eta) \in [\rho_{\min}, \rho_{\max}], \quad \tilde{U}(\eta) \in [u_{\min}, u_{\max}], \quad \tilde{W}(\eta) \in [w_{\min}, w_{\max}]. \tag{4.34a}$$

with

$$\rho_{\max} = \tilde{\rho}(\eta_0)\eta_0^{c_l - sc_l}(\eta_0 + h)^{sc_l - c_l}, \qquad \rho_{\min} = \tilde{\rho}(\eta_0)\eta_0^{3+c_l}(\eta_0+h)^{-3-c_l}, \tag{4.34b}$$

$$u_{\min} = \tilde{U}(\eta_0), \qquad w_{\max} = \tilde{W}(\eta_0) + \frac{s^2 c_l \rho_{\max}(\eta_0+h)h}{c_l - 2}, \tag{4.34c}$$

$$u_{\max} = \tilde{U}(\eta_0) + w_{\max}h, \qquad w_{\min} = \tilde{W}(\eta_0) - h\frac{w_{\max}}{\eta_0}(1 + \frac{c_l}{c_l + u_{\min}}). \tag{4.34d}$$

Proof. According to (4.6a) and the lower bound of $\tilde{U}(\eta)$ (3.7), we have

$$\tilde{\rho}'(\eta) \leq \frac{\tilde{\rho}(\eta)}{\eta}(sc_l - c_l), \quad \tilde{\rho}'(\eta) \geq \frac{\tilde{\rho}(\eta)}{\eta}(-3 - c_l). \tag{4.35}$$

By direct integration, we can get $\rho_{\max}$ and $\rho_{\min}$. Since $\tilde{U}(\eta)$ is increasing according to (4.6c), so we get the lower bound $u_{\min}$. Then using the upper bound $\rho_{\max}$ and the lower bound of $\tilde{U}(\eta)$ (3.7) in (4.6b), we get

$$\tilde{W}'(\eta) \leq \frac{s^2 c_l \rho_{\max}(\eta_0 + h)}{c_l - 2}. \tag{4.36}$$

By direct integration we get the upper bound $w_{\max}$. Putting the upper bound of $\tilde{W}(\eta)$ in (4.6c), we get the upper bound of $\tilde{u}(\eta)$, $u_{\max}$. Using the upper bound $w_{\max}$ and lower bound $u_{\min}$ in (4.6b), we have

$$\tilde{W}'(\eta) \geq \frac{w_{\max}}{\eta_0}(-1 - \frac{c_l}{c_l + u_{\min}}), \tag{4.37}$$

and with this we can get the lower bound of $\tilde{W}(\eta)$, $w_{\min}$. □

Using $|y_n - \tilde{y}_n| \leq E_n$ Lemma 4.3 and Lemma 4.2, we can get lower and upper bounds of y_n. Putting these the upper and lower bounds in (4.34), and using the same strategy as *Step 2*, we can get lower and upper bounds of the solutions on the interval $[x_n, x_{n+1}]$. Finally using these lower and upper bounds of the solutions in (4.33) and using the same strategy as in *Step 2*, we can rigorously bound I_2 using only floating point operation.

Step 6 The last part we need to control is I_3. I_3 is the roundoff error e_{roundoff} in updating $\tilde{y}_{n+1}$ using (4.26a). Using Lemma 4.3 and Lemma 4.2 and the same strategy as *Step 2*, we can get lower and upper bounds of the exact numerical solutions at the $n+1$-th step using only floating point operation. In our computation we use the upper bounds as our numerical solutions at $n+1$-th step, then the roundoff error introduced in this step can be bounded by the difference between the lower and upper bounds. So using Lemma 4.3 and Lemma 4.2 we can get upper bound of I_3 using only floating point operation.

Step 7 Putting the three parts of error bounds together and using Lemma 4.3 and Lemma 4.2, we get a rigorous error bound in the next step E_{n+1} using only floating point operation.

Step 8 Keep updating $\tilde{y}_n$ and E_n following *Steps 3-7*, we finally get the numerical solution of (4.6) at $\eta_0 = 3$ and a rigorous error bound, which are

$$\tilde{U}(\eta_0) \approx -1.6116, \quad \tilde{W}(\eta_0) \approx 3.6921 \times 10^{-2}, \quad \tilde{\rho}(\eta_0) \approx 3.8422 \times 10^{-3}. \tag{4.38}$$

and

$$E_n \leq (5 \times 10^{-5}, 5 \times 10^{-4}, 5 \times 10^{-6})^T. \tag{4.39}$$

With these numerical solutions and the error bounds, we can easily verify that condition (4.1c) holds, and we complete the proof that for $s = 2$,

$$G(3) < 0. \tag{4.40}$$

4.2. **The case $s = 2$, c_l=8.** The verification of $G(8) > 0$ can be done in the same way. In the construction of the local solutions, we can easily verify the choice of

$$u^0 = \frac{1}{6}, \quad \rho^0 = \frac{1}{18}, \quad r = 6, \tag{4.41}$$

makes the constraint (2.10) hold. Then we truncate the power series (2.1) to the first 20 terms and evaluate them at $\xi = 0.6^8$, corresponding to $\eta_s = 0.6$. Using the same technique as the case $c_l = 3$, we can get the approximated profiles and error bounds at η_s,

$$\tilde{y}_0, \quad E_0 = (10^{-13}, 10^{-13}, 10^{-13})^T. \tag{4.42}$$

Then we begin to solve (4.6). Using the same technique as the previous case to bound the numerical error in solving the ODE system, we finally get

$$\tilde{U}(3) \approx 4.7661 \times 10^{-1}, \tag{4.43}$$

with numerical error bounded by

$$E_n^u \leq 2 \times 10^{-2}. \tag{4.44}$$

Then (4.1a) holds and we complete the proof that for $s = 2$,

$$G(8) > 0. \tag{4.45}$$

With $G(3) < 0$, $G(8) > 0$, we conclude that there exists a c_l such that the self-similar equations have solutions, and the leading order of $\rho(\xi)$ at $\xi = 0$ is $s = 2$.

Following the same procedure we also verified that for

$$s = 3, 4, 5, \tag{4.46}$$

there exists c_l such that the self-similar equations have solutions. We omit the numerical details here for clarity. Now we complete the proof of Theorem 1.1, i.e. there exist a family of self-similar profiles corresponding to different leading orders of $\rho(\xi)$, $s = 2, 3, 4, 5$.

Remark 4.2. *We only verify the existence of self-similar profiles for $s = 2, 3, 4, 5$. But the same procedure can be applied to $s > 5$ to verify the existence of self-similar profiles.*

5. Behavior of the Self-Similar Profiles at Infinity

In this section, we prove that if the decay condition (1.8b) in the Biot-Savart law is satisfied for the self-similar profiles we construct, then the profiles are actually analytic with respect to a transformed variable $\theta = \xi^{-1/c_l}$ at $\theta = 0$. With this we can complete the proof of Theorem 1.2. This far-field property of the profiles can explain the Hölder continuity of the velocity field at the singularity time observed in numerical simulation of this model.

Theorem 5.1. *For some fixed c_l and s, if the self-similar profiles constructed using power series (2.1) and extended to whole R^+ satisfy the decay condition (1.8b), then after the following change of variables,*

$$\theta = \xi^{-1/c_l}, \quad \tilde{U}(\theta) = U(\xi)\xi^{-1+1/c_l}, \quad \tilde{\rho}(\theta) = \rho(\xi)\xi^{-1+2/c_l}, \quad \tilde{W}(\theta) = W(\xi)\xi^{1/c_l}, \tag{5.1}$$

$\tilde{U}(\theta)$, $\tilde{W}(\theta)$ and $\tilde{\rho}(\theta)$ are analytic functions at $\theta = 0$.

Our strategy is the following: We first prove that after the change of variables (5.1), $\tilde{U}(\theta)$, $\tilde{W}(\theta)$ and $\tilde{\rho}(\theta)$ are smooth at $\theta = 0$. Then we argue that there exist analytic solutions to the ODE system they satisfy with the same initial conditions at $\theta = 0$. Finally we prove that smooth solutions with given initial conditions are unique and complete the proof.

Proof. If the decay condition (1.8b) holds, $\hat{U}(\eta)$ tends to 0 in equation (3.6), so there exists $\eta_0 > 0$ such that for $\eta > \eta_0$,

$$\frac{(2/c_l - 1)\hat{U}(\eta)}{1 + 1/c_l\hat{U}(\eta)} \in (0, 1/2). \tag{5.2}$$

Then based on (3.6a), we have for $\eta > \eta_0$,

$$\hat{\rho}'(\eta) \le \frac{1/2\hat{\rho}(\eta)}{\eta}, \tag{5.3}$$

which implies that for $\eta > \eta_0$,

$$\hat{\rho}(\eta) \le C_1\eta^{1/2}. \tag{5.4}$$

Using this estimate in (3.6b), we have for $\eta > \eta_0$,

$$\big(\hat{W}(\eta)\eta\big)' \le C_2\eta^{-3/2}, \tag{5.5}$$

which gives

$$\hat{W}(\eta)\eta < C_3. \tag{5.6}$$

Using the above estimate in (3.6c), we get for $\eta > \eta_0$,

$$\hat{U}'(\eta) \le C_4\eta^{-2}, \tag{5.7}$$

which together with $\hat{U}(+\infty) = 0$ implies that for $\eta > \eta_0$,

$$\hat{U}(\eta) \le C_5\eta^{-1}. \tag{5.8}$$

Based on (3.6b) and (3.6c), we have

$$\hat{\rho}'(\eta) = \frac{(2/c_l - 2)\hat{\rho}(\eta)\hat{U}(\eta)}{\eta + 1/c_l\hat{U}(\eta)\eta}, \quad (\hat{W}(\eta)\eta)' = \frac{1/c_l\hat{U}(\eta)\hat{W}(\eta)}{1 + 1/c_l\hat{U}(\eta)} + \frac{(1 - 2/c_l)\hat{\rho}(\eta)}{(1 + 1/c_l\hat{U}(\eta))^2\eta^2}. \tag{5.9}$$

Using (5.8) and (5.4) in (5.9), we can see that $|\hat{\rho}'(\eta)|$ and $|(\hat{W}(\eta)\eta)'|$ are both integrable from η_0 to $+\infty$, thus $\hat{\rho}(\eta)$ and $\hat{W}(\eta)\eta$ converge as $\eta \to +\infty$.

$$\lim_{\eta\to\infty} \hat{W}(\eta)\eta = \hat{W}_\infty \in [0, +\infty), \quad \lim_{\eta\to\infty} \hat{\rho}(\eta) = \hat{\rho}_\infty \in (0, +\infty). \tag{5.10}$$

Then based on (3.6c), and the fact that $\hat{U}(+\infty) = 0$, we have

$$\lim_{\eta\to+\infty} \hat{U}(\eta)\eta = c_l\hat{W}_\infty. \tag{5.11}$$

The above limits imply that after changing variables, $\tilde{U}(\theta)$, $\tilde{\rho}(\theta)$ and $\tilde{W}(\theta)$ are continuous for $\theta \in [0, +\infty)$. The ODE system they satisfy for $\theta \in (0, +\infty)$ is

$$\tilde{\rho}'(\theta) = \frac{(2/c_l - 1)\tilde{\rho}(\theta)\tilde{U}(\theta)}{-1 - \tilde{U}(\theta)\theta}, \tag{5.12a}$$

$$\tilde{W}'(\theta) = \frac{1/c_l\tilde{U}(\theta)\tilde{W}(\theta) + (1 - 2/c_l)\tilde{\rho}(\theta) - 1/c_l\tilde{\rho}'(\theta)\theta}{-1 - \tilde{U}(\theta)\theta}, \tag{5.12b}$$

$$\tilde{U}'(\theta) = -\frac{\tilde{U}(\theta)}{\theta} - \frac{c_l\tilde{W}(\theta)}{\theta}, \tag{5.12c}$$

with initial conditions given by (5.10) and (5.11).

$$\tilde{W}(0) = \hat{W}_\infty, \quad \tilde{\rho}(0) = \hat{\rho}_\infty, \quad \tilde{U}(0) = c_l\hat{W}_\infty. \tag{5.12d}$$

Equation (5.12c) can be written as

$$\tilde{U}(\theta) = \frac{c_l}{\theta}\int_0^\theta \tilde{W}(\zeta)\mathrm{d}\zeta. \tag{5.13}$$

Using a simple bootstrap argument, we can get $\tilde{W}(\theta)$, $\tilde{\rho}(\theta)$ and $\tilde{U}(\theta)$ are in $C^\infty\big([0,+\infty)\big)$. On the other hand, given the initial conditions (5.12d), we can construct the following power series solutions to equations (5.12):

$$\tilde{U}(\theta) = c_l\hat{W}_\infty + \sum_{k=1}^{\infty}\tilde{U}_k\theta^k, \quad \tilde{W}(\theta) = \hat{W}_\infty + \sum_{k=1}^{\infty}\tilde{W}_k\theta^k, \quad \tilde{\rho}(\theta) = \hat{\rho}_\infty + \sum_{k=1}^{\infty}\tilde{\rho}_k\theta^k. \tag{5.14}$$

Plugging these power series ansatz in (5.12) and matching the coefficients of θ^k, we can uniquely determine the coefficients $\tilde{U}_k$, $\tilde{W}_k$, $\tilde{\rho}_k$ and prove that the power series (5.14) converge in a small neighborhood of $\theta = 0$. We omit the details here, because the argument are the same as in section 2. Then to prove the analyticity of $\tilde{U}(\theta)$, $\tilde{W}(\theta)$ and $\tilde{\rho}(\theta)$ at $\theta = 0$, we only need the uniqueness of smooth solutions to (5.12) with initial condition (5.12d). The RHS of (5.12c) is not Lipschitz continuous, so the classical result will not apply here.

Assume $\tilde{U}^i(\theta)$, $\tilde{W}^i(\theta)$, $\tilde{\rho}^i(\theta)$, $i = 1, 2$, are two different solutions to equation (5.12) with initial condition (5.12d). And let $\delta U(\theta)$, $\delta W(\theta)$, $\delta\rho(\theta)$ be the difference of the two solutions,

$$\delta\tilde{U}(\theta) = \tilde{U}^1(\theta) - \tilde{U}^2(\theta), \quad \delta\tilde{W}(\theta) = \tilde{W}^1(\theta) - \tilde{W}^2(\theta), \quad \delta\tilde{\rho}(\theta) = \tilde{\rho}^1(\theta) - \tilde{\rho}^2(\theta). \tag{5.15}$$

Then based on (5.12c),

$$\delta U(\theta) = \frac{c_l}{\theta}\int_0^\theta \delta W(\zeta)\mathrm{d}\zeta. \tag{5.16}$$

Using hardy inequality[6], there exists C_1 independent of ϵ such that

$$\|\delta\tilde{U}\|_{L^2([0,\epsilon])} \le C_1\|\delta\tilde{W}\|_{L^2([0,\epsilon])}. \tag{5.17}$$

Since the right hand side of (5.12a) and (5.12b) are Lipschitz continuous, we have

$$|\frac{\mathrm{d}}{\mathrm{d}\theta}(\delta\tilde{W}(\theta))| + |\frac{\mathrm{d}}{\mathrm{d}\theta}(\delta\tilde{\rho}(\theta)))| \le C_2(|\delta\tilde{W}(\theta)| + |\delta\tilde{U}(\theta)| + |\delta\tilde{\rho}(\theta)|) \tag{5.18}$$

Integrating the square of both sides on the interval $[0, \epsilon]$ and using (5.17), we get

$$\|\big(\delta\tilde{W}(\theta)\big)'\|_{L^2([0,\epsilon])} + \|\big(\delta\tilde{\rho}(\theta)\big)'\|_{L^2([0,\epsilon])} \le C_3(\|\delta\tilde{W}(\theta)\|_{L^2([0,\epsilon])} + \|\delta\tilde{\rho}(\theta)\|_{L^2([0,\epsilon])}). \tag{5.19}$$

Since $\delta\tilde{W}(\theta)$ and $\delta\tilde{\rho}(\theta)$ vanish on $\theta = 0$, by Poincaré-Friedrichs inequality we have

$$\|\delta\tilde{W}(\theta)\|_{L^2([0,\epsilon])} + \|\delta\tilde{\rho}(\theta)\|_{L^2([0,\epsilon])} \le C_4\epsilon(\|\big(\delta\tilde{W}(\theta)\big)'\|_{L^2([0,\epsilon])} + \|\big(\delta\tilde{\rho}(\theta)\big)'\|_{L^2([0,\epsilon])}). \tag{5.20}$$

The C in the above estimates are all positive constants independent of ϵ. Choosing ϵ small enough, we get a contradiction in (5.19) and (5.20), thus

$$\tilde{W}^1 = \tilde{W}^2, \quad \tilde{U}^1 = \tilde{U}^2, \quad \tilde{\rho}^1 = \tilde{\rho}^2, \tag{5.21}$$

which means the solution is unique. And we complete the proof of this Theorem. □

The above Theorem implies the self-similar profiles we construct are non-conventional in the sense that the velocity does not decay to 0 at $+\infty$ but grows with certain fractional power. Coming back to the self-similar ansatz (1.4), we have

$$u(x,t) = (T-t)^{c_l-1}U\left(\frac{x}{(T-t)^{c_l}}\right). \tag{5.22}$$

For t close to T, based on Theorem 5.1 , we have

$$u(x,t) \approx C(T-t)^{c_l-1}\frac{x}{(T-t)^{c_l}}\left(\frac{x}{(T-t)^{c_l}}\right)^{-\frac{1}{c_l}} = Cx^{1-\frac{1}{c_l}}. \tag{5.23}$$

This can explain the Hölder continuity of the velocity field near singularity time, which is observed in simulation of the 1D model. Such behavior is also observed in the numerical computation of the 3D Euler equations in [8], which is very different from the Leray type of self-similar solutions of the 3D Euler equations, whose existence has been ruled out under certain decay assumptions on the self-similar profiles [2, 1, 3].

6. Numerical Results

In this section we numerically locate c_l which makes $G(c_l) = 0$ for several different s and construct the corresponding self-similar profiles. The scaling exponents and self-similar profiles obtained from solving the self-similar equations (1.6) agree with those obtained from direct numerical simulation of the CKY model. We also find that for fixed s, the singular solutions using different initial conditions converge to the same self-similar profiles after rescaling, which means the self-similar profiles we find have some stability property.

6.1. Numerical methods for solving the self-similar equations.

For any fixed $c_l > 2$, we first numerically compute the coefficients ρ_k, U_k in (2.1) up to $k = 50$ and determine the convergence radius of the power series using the following linear regression for $s \le k \le 50$,

$$\log \rho_k = k \log r_1 + c_1, \quad \log U_k = k \log r_2 + c_2. \tag{6.1}$$

We choose

$$r = \frac{1}{2}\min\{\frac{1}{r_1}, \frac{1}{r_2}\}. \tag{6.2}$$

and construct the local self-similar profiles on $[0, r/2]$.

Then we continue solving equation (1.6) from $\xi = r/2$ to $\xi = 1$ using the 4th order explicit Runge-Kutta method with step-size $h = \frac{1-r/2}{10^4}$. After $\xi = 1$, we make the change of variables (3.4) and begin to solve (3.6) from $\eta = 1$ to $\eta = 10^5$ using 4th order Runge-Kutta method with step-size $h = \frac{10^5-1}{10^6}$. We use $\hat{U}_{c_l}(10^5)$ as an approximation to $G(c_l)$.

We use the bisection method to find the root of $G(c_l)$, and the stopping criterion is that the length of the subinterval becomes less than 10^{-5}. After we get the scaling exponent c_l, we construct the local self-similar profiles using power series (2.1) as before and numerically extend them from $\xi = r/2$ to $\xi = 10$ using the explicit 4th order Runge-Kutta method with step-size $h = \frac{9}{10^4}$. Then we locate the maxima of W, which is $W_{\max} = W(\xi_0)$. We consider $s = 2, 3, 4, 5$, and for these cases ξ_0 are all less than 10. Finally we rescale the maximum of the $W(\xi)$ to $(1, 1)$, and get the rescaled self-similar profile of w

$$W_s(\xi) = \frac{1}{W_{\max}} W(\xi\xi_0), \quad \xi \in [0, 1]. \tag{6.3}$$

We will only compare the self-similar profiles of W_s with direct simulation of the CKY model in this paper, but the numerical results for the profiles of ρ and U are similar.

6.2. **Numerical methods for simulating the model.** In the direct simulation of the CKY model, we use a particle method. We consider $N+1$ particles with position, density and vorticity given by

$$\begin{cases} q = (q_0(t), q_1(t), \dots q_N(t))^T, \\ \rho = (\rho_0(t), \rho_1(t), \dots \rho_N(t))^T, \\ w = (w_0(t), w_1(t), \dots w_N(t))^T. \end{cases} \tag{6.4}$$

In computing the velocity field, we use the trapezoidal rule to approximate (1.6c),

$$u_i = -q_i \left(\sum_{j=i}^{N-1} \frac{w_j + w_{j+1}}{2} (q_{j+1} - q_j) \right). \tag{6.5}$$

In computing the driving force of w, which is ρ_x, we use the three points rule:

$$(\rho_x)_i = \begin{cases} 0, & i = 0, \\ \frac{\rho_i - \rho_{i+1}}{q_i - q_{i+1}} + \frac{\rho_i - \rho_{i-1}}{q_i - q_{i-1}} + \frac{\rho_{i+1} - \rho_{i-1}}{q_{i+1} - q_{i-1}}, & 0 < i < N, \\ \frac{\rho_i - \rho_{i-2}}{q_i - q_{i-2}} + \frac{\rho_i - \rho_{i-1}}{q_i - q_{i-1}} + \frac{\rho_{i-2} - \rho_{i-1}}{q_{i-2} - q_{i-1}}, & i = N. \end{cases} \tag{6.6}$$

Initially, 10^5+1 particles are equally put in the short interval $[0, 10^{-3}]$, which are sufficient to resolve the solutions in the self-similar regime. Outside this short interval $10^5 - 10^2$ particles are equally placed with distance 10^{-5}. So the total number of particles is $N = 2 \times 10^5 - 10^2$.

Then we need to solve the following ODE system

$$\frac{\mathrm{d}}{\mathrm{d}t} q = u, \quad \frac{\mathrm{d}}{\mathrm{d}t} w = \rho_x, \quad \frac{\mathrm{d}}{\mathrm{d}t} \rho = 0. \tag{6.7}$$

The initial condition of ρ is

$$\rho(x, 0) = (1 - \cos(\pi x))^{s/2}, \tag{6.8}$$

whose leading order at $x = 0$ is s.

We solve the ODE system 6.7 using the 4-th order explicit Runge-Kutta method, and the time step dt is chosen adaptively to avoid the particles cross each other:

$$dt_i = \frac{1}{\max(\frac{u_i - u_{i+1}}{q_{i+1} - q_i}, 0)}, \quad dt = \min(\frac{dt_i}{10}, 10^{-3}). \tag{6.9}$$

Simulation of this model will stop once the maximal vorticity reaches some preset $W_{\max}$. And at each time step, we record the maximal vorticity $w_{\max}(t_i)$, and the position where it is attained $q_{\max}(t_i)$. According to the self-similar ansatz, we have

$$w_{\max}(t) = C_1 (T - t)^{c_w}, \quad q_{\max}(t) = C_2 (T - t)^{c_l}. \tag{6.10}$$

Thus we can compute c_l c_w, and the singularity time T by doing linear regression,

$$(\frac{\mathrm{d}}{\mathrm{d}t} \log w_{\max}(t))^{-1} \approx -\frac{1}{c_w} t + \frac{T}{c_w}, \tag{6.11a}$$

$$(\frac{\mathrm{d}}{\mathrm{d}t} \log q_{\max}(t))^{-1} \approx -\frac{1}{c_l} t + \frac{T}{c_l}. \tag{6.11b}$$

We compute the time derivatives of $\log w_{\max}(t)$ and $\log q_{\max}(t)$ using the center difference method, and the linear regressions are done in some time interval close to the singularity time while the numerical solutions still have good accuracy.

At certain time steps close to the singularity time, t^i, $i = 1, 2, 3$, let w^i be the maximal vorticity at time t^i and q^i be the position the maximal vorticity is attained. We rescale the numerical solution and get the self-similar profile of w,

$$W_s^i(\xi) = \frac{1}{w_{\max}} w(\xi q^i, t^i), \quad \xi \in [0, 1]. \tag{6.12}$$

In the next subsection we will compare the self-similar profiles $W_s^i(\xi)$ (6.12), which are obtained from direct simulation of the model, with $W_s(\xi)$ given by (6.3), which is obtained from solving the self-similar equations (1.6).

Near the singularity time the velocity field seems to be Hölder continuous near the origin,

$$u(x, T) \approx Cx^\alpha. \tag{6.13}$$

Then we can determine the Hölder exponent α by doing linear regression

$$\ln u(x, T) \approx \ln C + \alpha \ln x. \tag{6.14}$$

We will compare the exponents α we get from direct simulation of the CKY model with our prediction (5.23) obtained from analyzing the self-similar equations.

6.3. **Comparison results.** In our direct simulation of the CKY model, we first choose the initial condition of $w(x, t)$ as

$$w(x, 0) = 1 - \cos(4\pi x). \tag{6.15}$$

We compute the scaling exponents c_w and c_l for different leading orders of ρ, $s = 2, 3, 4, 5$ using direct simulation of the CKY model, and the results are listed in Table 1 and Table 2. We also compute the Hölder exponents of the velocity field near the origin at the singularity time and compare them with $1-1/c_l$ as predicted by (5.23). The results are listed in Table 3. The c_l we use are those obtained from solving the self-similar equations.

For $s = 2$, the linear regression (6.11a) and (6.11b) are done in the time interval

$$[6.4371 \times 10^{-1}, 6.4391 \times 10^{-1}], \tag{6.16}$$

and the predicted singularity time T for (6.11a) and (6.11b) are both 6.4402×10^{-1}. The linear regression (6.14) is done at $t = 6.4391 \times 10^{-1}$ and on the interval $[10^{-10}, 10^{-9}]$.

For $s = 3$, the linear regression (6.11a) and (6.11b) are done in the time interval

$$[6.804297 \times 10^{-1}, 6.804300 \times 10^{-1}], \tag{6.17}$$

and the predicted singularity time T for (6.11a) and (6.11b) are both 6.804302×10^{-1}. The linear regression (6.14) is done at $t = 6.804302 \times 10^{-1}$ and on the interval $[10^{-10}, 10^{-9}]$.

For $s = 4$, the linear regression (6.11a) and (6.11b) are done in the time interval

$$[6.571218 \times 10^{-1}, 6.571221 \times 10^{-1}], \tag{6.18}$$

and the predicted singularity time T for (6.11a) and (6.11b) are both 6.571223×10^{-1}. The linear regression (6.14) is done at $t = 6.571223 \times 10^{-1}$ and on the interval $[10^{-10}, 10^{-9}]$.

For $s = 5$, the linear regression (6.11a) and (6.11b) are done in the time interval

$$[5.9698511 \times 10^{-1}, 5.9698515 \times 10^{-1}], \tag{6.19}$$

and the predicted singularity time T for (6.11a) and (6.11b) are both 5.9698517×10^{-1}. The linear regression (6.14) is done at $t = 5.9698517 \times 10^{-1}$ and on the interval $[10^{-10}, 10^{-9}]$.

From the Table 1, 2 3, we can see that the exponents c_w we obtain from the singular numerical solutions are close to -1 (1.5). The c_l we obtain from direct simulation of this model

	$s=2$	$s=3$	$s=4$	$s=5$
c_w	-0.9747	-1.0001	-1.0006	-1.0007

TABLE 1. c_w table

	$s=2$	$s=3$	$s=4$	$s=5$
CKY	3.7942	3.3143	3.1718	3.0773
Self-Similar	3.7967	3.3157	3.1597	3.0841

TABLE 2. c_l table

	$s=2$	$s=3$	$s=4$	$s=5$
Hölder exponent	7.3381×10^{-1}	6.9823×10^{-1}	6.9131×10^{-1}	6.7610×10^{-1}
$1-1/c_l$	7.3661×10^{-1}	6.9841×10^{-1}	6.8351×10^{-1}	6.7576×10^{-1}

TABLE 3. Hölder exponent of the velocity field at 0 and $1-1/c_l$.

are close to those obtained from solving the self-similar equations. And at the singularity time the Hölder exponents of the velocity field are close to $1-1/c_l$.

For the case $s=2$, the dependence of $G(c_l)$ on c_l is plotted in Figure (1). From this Figure, we can see that $G(c_l)$ depends continuously on c_l as we have proved. Besides, $G(c_l)$ seems to be a monotone increasing function, which implies that for fixed s, the scaling exponent c_l to make the decay condition (1.8b) hold is unique.

.

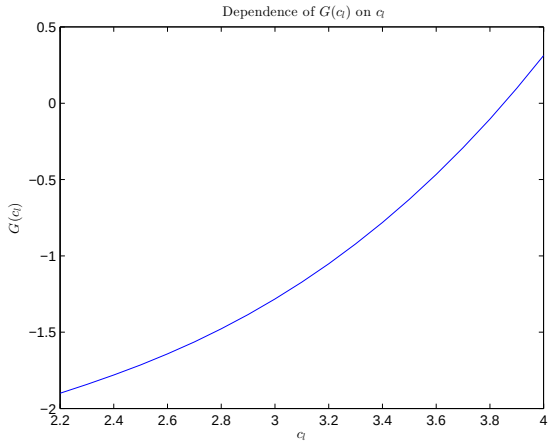

FIGURE 1. Dependence of $G(c_l)$ on c_l for $s=2$

We also compare the self-similar profiles obtained from solving (1.6) and those obtained from direct simulation of the model. For different s, they are plotted in Figure 2. The lines labeled 'exact' are obtained from solving the self-similar equation. Others are obtained from rescaling the solution at different time steps corresponding to different maximal vorticity.

To demonstrate the stability the self-similar profiles, we consider another initial condition,

$$w(x,0)=x-x^2. \tag{6.20}$$

Again we compare the self-similar profiles of w from direct simulation of the model with those obtained from solving the self-similar equations (1.6). They are plotted in Figure 3.

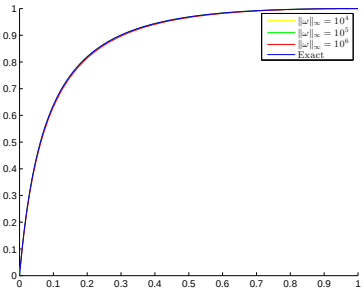

(A) The re-scaled solutions and self-similar profiles we construct. $s = 2$.

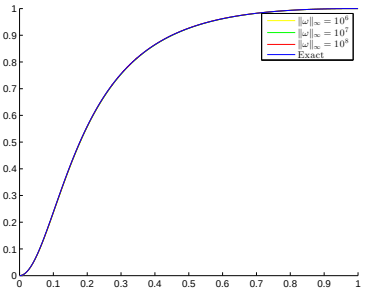

(B) The re-scaled solutions and self-similar profiles we construct. $s = 3$.

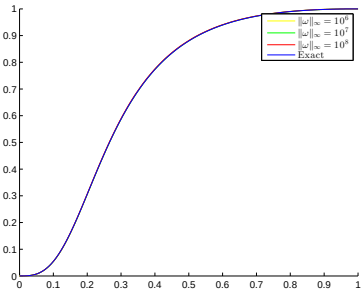

(C) The re-scaled solutions and self-similar profiles we construct. $s = 4$.

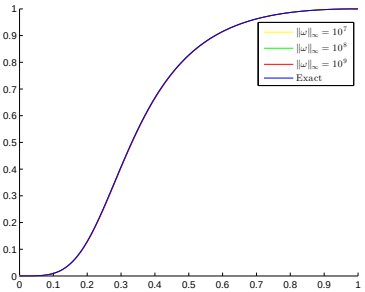

(D) The re-scaled solutions and self-similar profiles we construct. $s = 5$.

FIGURE 2. Self-similar profiles of w using initial condition $w(x, 0) = 1 - \cos(4\pi x)$.

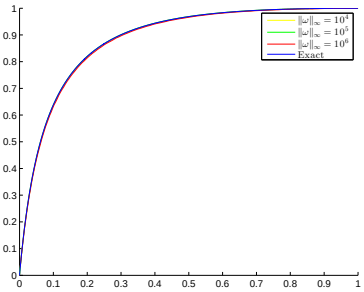

(A) $s = 2$

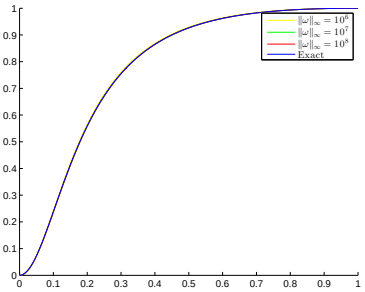

(B) $s = 3$

FIGURE 3. Self-similar profiles of w using initial condition $w(x, 0) = x - x^2$.

From Figure 2, 3, we can see that after rescaling, the singular solutions at different time steps before the singularity time are very close, which implies that the solutions of this 1D model develop self-similar singularity. And the self-similar profiles obtained from direct simulation of the model (6.12) agree very well with the self-similar profiles we construct (6.3) by sovling the self-similar equations (1.6). For fixed leading order of $\rho(x, 0)$ at the origin, the singular solutions with different initial conditions converge to the same set of self-similar profiles, which implies that the profiles we construct have some stability property.

Acknowledgements. The authors would like to thank Professors Russel Caflisch and Guo Luo for a number of stimulating discussions. We would also like to thank Professors

Alexander Kiselev and Yao Yao for their interest in our work and for their valuable comments. The research was in part supported by NSF FRG Grant DMS-1159138.

References

[1] Dongho Chae. Nonexistence of asymptotically self-similar singularities in the euler and the navier–stokes equations. *Mathematische Annalen*, 338(2):435–449, 2007.

[2] Dongho Chae. Nonexistence of self-similar singularities for the 3d incompressible euler equations. *Communications in Mathematical Physics*, 273(1):203–215, 2007.

[3] Dongho Chae. On the self-similar solutions of the 3d euler and the related equations. *Communications in Mathematical Physics*, 305(2):333–349, 2011.

[4] Kyudong Choi, Thomas Y. Hou, Alexander Kiselev, Guo Luo, Vladimir Sverak, and Yao Yao. On the fiinite-time blowup of a 1d model for the 3d axisymmetric euler equations. *arXiv preprint arXiv:1407.4776*, 2014.

[5] Kyudong Choi, Alexander Kiselev, and Yao Yao. Finite time blow up for a 1d model of 2d boussinesq system. *arXiv preprint arXiv:1312.4913*, 2013.

[6] D.J.H. Garling. *Inequalities: a journey into linear analysis*, volume 19. Cambridge University Press Cambridge, 2007.

[7] John D Gibbon. The three-dimensional euler equations: Where do we stand? *Physica D: Nonlinear Phenomena*, 237(14):1894–1904, 2008.

[8] Thomas Y Hou and Guo Luo. On the finite-time blowup of a 1d model for the 3d incompressible euler equations. *arXiv preprint arXiv:1311.2613*, 2013.

[9] Alexander Kiselev and Vladimir Sverak. Small scale creation for solutions of the incompressible two dimensional euler equation. *arXiv preprint arXiv:1310.4799*, 2013.

[10] Guo Luo and Thomas Y Hou. Potentially singular solutions of the 3d incompressible euler equations. *arXiv preprint arXiv:1310.0497*, 2013.

[11] Andrew J Majda and Andrea L Bertozzi. *Vorticity and incompressible flow*, volume 27. Cambridge University Press, 2002.

[12] Dan Zuras, Mike Cowlishaw, Alex Aiken, Matthew Applegate, David Bailey, Steve Bass, Dileep Bhandarkar, Mahesh Bhat, David Bindel, Sylvie Boldo, et al. Ieee standard for floating-point arithmetic. *IEEE Std 754-2008*, pages 1–70, 2008.